DYNAMIC RESPONSE ANALYSIS OF SUBMERGED FLOATING TUNNELS UNDER HYDRODYNAMIC LOADS AND SEISMIC EXCITATIONS

A Thesis

by

JOOYOUNG LEE

Submitted to the Office of Graduate and Professional Studies of
Texas A&M University
in partial fulfillment of the requirements for the degree of

MASTER OF SCIENCE

Chair of Committee,	Moo-Hyun Kim
Committee Members,	Robert E. Randall
	Achim Stössel
Head of Department,	Sharath Girimaji

May 2017

Major Subject: Ocean Engineering

ABSTRACT

This thesis presents the numerical simulation results for a submerged floating tunnel (SFT) under hydrodynamic loads and seismic excitation. Time domain simulations are conducted via OrcaFlex and CHARM3D. SFTs with either vertical and inclined mooring lines were evaluated. The SFTs are assumed to have rigid body, and a Morison equation is used to calculate hydrodynamic loads on SFT. Regular and irregular waves are used in the simulations. In particular, the results of the numerical mockup of the regular wave condition is compared with the experimental conditions for validation of the numerical model. Furthermore, regular and real excitation data are applied to the anchor points of the mooring lines to simulate SFTs under seismic loads; also surge, heave, and mooring tensions are all compared. Different trends are obtained between the hydrodynamic and seismic effects. In the hydrodynamic loads, the motion of SFTs with vertical mooring line is more significant than the motion of those with inclined mooring line. Whereas, in seismic displacement conditions, the motion of SFTs with inclined mooring line is more significant than the motion of SFTs with vertical mooring line. Tension in SFT with vertical mooring line is greater than the tension in SFT with inclined mooring line. These results represent the unique behavior of SFTs under seismic excitation when compared with wave conditions, and suggest the SFT concept for seismic situations.

DEDICATION

To my parents, Byung-Sang Lee and Mi-Youn Kang, and my sister and bother, Yu-Min Lee and Do-Hyun Lee,

with Love

ACKNOWLEDGEMENTS

I would like to express my deepest appreciation to my advisor, Dr. Moo-Hyun Kim, who provided his kind guidance and tireless assistance throughout my research. He is my role model, both personally and professionally.

Special thanks are also extended to Dr. Robert Randall and Dr. Achim Stössel for their excellent assistance as my committee advisors.

Additionally, I am so grateful to all of my colleagues who supported me and offered me the tremendous gift of their friendship at this stage in my life.

Finally, I would like to express my sincere appreciation to my parents, Byung-Sang Lee and Mi-Youn Kang, as well as to my sister, Yu-Min Lee, and my brother, Do-Hyun Lee, for their love and encouragement throughout this process.

CONTRIBUTORS AND FUNDING SOURCES

This thesis was supervised by a thesis committee consisting of Professor Moo-hyun Kim and Robert E. Randall of the Department of Ocean Engineering and Professor Achim Stössel of the Department of Oceanography.

All work for the thesis was completed independently by the student, under the advisement of Moohyun Kim of the Department of Ocean Engineering.

Graduate study was supported by a scholarship from Texas A&M University.

TABLE OF CONTENTS

Page

LIST OF FIGURES

LIST OF TABLES

CHAPTER I

INTRODUCTION

Many countries considered a Submerged Floating Tunnel (SFT) to lessen their limitation of geographical features. In Norway and Italy, SFTs are a new type of solution used to overcome their geographical restrictions by connecting fjords or straits. Furthermore, some locations in Asia, including South Korea, China and Japan, implement SFTs as an alternative form of transportation, connecting each other while saving travel money and time. The interest for SFTs was revived in the 1960's with some minor research and many countries; Norway, Italy, and Japan, started this effort of increased interest (Østlid, 1877). However, the deep depth of water, long distances, and other challenging environmental conditions make connecting land points across fjords and straits difficult. There are four typical forms of Submerged Floating Tunnels: pontoons, column support, tension leg, and free (Østlid, 1877). The different types of SFTs should be installed according to the region and geographical features of ocean.

The most significant strengths of SFTs are the structural and environmental abilities and economic feasibility. Recently, the Norwegian Public Roads Administration (NPRA) has proposed the first SFT to provide connection across a fjords. The west side of Norway features more than thousand fjords, making travelling difficult and time consuming. The current drive time between the northern and southern cities of Kristiansand and Trondheim takes about twenty-one hours. The NPRA is considering SFTs as a means of saving travel time. The tunnel will be 4000 feet long and 66 feet below

the surface of the Norwegian Sea. Following Norway's decision, many countries have gained interest in SFTs and are trying to find feasible opportunities. Because this type of structure has never been created until now, many engineers are challenged to better understand and consider the concept before actively responding.

Diverse scenarios have been analyzed under multiple load conditions in order to design and install a SFT structure. To determine the realistic potential of SFTs, various analysis techniques should be developed and tested by engineers to demonstrate the dynamic behaviors of the structure. Dean (1948) performed the first analysis, and its results determined the interaction between sea waves and a submerged horizontal circular cylinder in deep water. Until now, many researchers have investigated the effects of random waves on SFTs. However, since natural disasters have increased around the world due to environmental changes, they should not be overlooked. Furthermore, the effects of environmental disasters such as earthquakes must also be investigated, as well as effects of the ocean's wave forces. Since the Kobe earthquake in 1995, researchers have been increasingly attentive to seismic resistance of underground structures through analysis and numerical methods. However, the research about the dynamic response of underground tunnels in seismic conditions have not been studied (Cheng, 2014). Completing research about the dynamic response of SFTs under seismic excitation is a critical part of its implementation. Several researches have been done about behavior of SFT with seismic.

In this study, the modeling and numerical analysis of a SFT and mooring line under seismic excitation is investigated through OrcaFlex and CHARM 3D using a time domain. The design concepts of SFTs is evaluated based on its motion characteristics of SFT with

both vertical and inclined mooring lines. For this study, the Morison equation force, which describes fluid motion, was used to calculate the hydrodynamic load and motion of structures under the seismic excitation with a time series of seismic motion. The drag and inertia forces must be simultaneously used for calculating the wave loading on a submerged tunnel. However, if the diameter of a tunnel is too large, the inertia force is more dominant than the drag force. Thus, to calculate the wave force, the SFT can either use the Morison force method or the Boundary Element Method (Kunisu, 2010). For modeling conditions of Orcaflex, soil-structure interaction is ignored and hydrodynamic force due to rigid body structure. Although the same formulation is used for tunnel and mooring lines in OrcaFlex and CHARM3D, a lumped mass element is considered for rigid body mass to simplify the mathematical formulation in OrcaFlex and the mooring lines in CHARM3D are discretized using a FEM(Finite Element Method) approach proposed by Garrett (1982). In this modeling process, the perpendicular traveling wave to the axial direction of the tunnel is used for regular wave, while the JONSWAP spectrum with γ 3.3 is used for irregular wave. Real time history displacement records are used for seismic excitation source. Under two hydrodynamic conditions, regular wave and irregular wave, the results of SFT dynamic responses from OrcaFlex are obtained to validate and compared with CHARM3D. Furthermore, the dynamic motion of SFT was retrieved to estimate the trend under the seismic excitation. Through this numerical analysis, this research was able to derive the dynamic responses of SFT motion in relation to the two above-mentioned types of mooring lines.

CHAPTER II

LITERATURE REVIEW

There have been various studies with respect to dynamic response of submerged floating tunnel under seismic conditions. Brancaleoni (1989) investigated dynamic response of two different types of SFT, short span with cable anchors and long span with rigid pier supports, under sea wave or seismic conditions. And they suggest the appropriately formulation to investigate the motion of SFTs under incident wave and seismic wave conditions. Fogazzi et al. (2000) and Di Pilato et al. (2008) studied behavior of SFT as the multi-supported structure with seismic effects and developed influence of interaction between structure and ground with simplified procedure. Fogazzi used the two different non-linear SFTs design with different inclined anchor element and numerical simulation, ABAQUS, for this research. They assumed the charateristics of soil is linear and the interation effect of soil and structure are analyzed as mean of lumped-parameter approach. Remseth et al. (1999) employed the finite element method to demonstrate the interaction between SFTs and wave loading, as well as the effects of force, damping, and tension on SFTs. The non-stationary responses of suspension bridges with multiple supports SFT under earthquake ground excitation was investigated by Hyun et al. (1992). The results induced that the effect of a horizontal seismic motion was more significant than a vertical motion. Chen and Huang (2010) studied the dynamic characteristics of a SFT by conducting a numerical analysis of the seismic wave passage effect. SFT with the multi-support excitation were also evaluated through the large mass method. The study

showed the multi-support seismic excitation has strong influence about dynamic responses of submerged floating tunnel. They use real velocity time series, show maximum transverse moments, and shear force response under the multi-support excitation. The most significant responses of structure occur at the far right of the tunnel. This finding reflects the unique behavior of SFTs under the multi-support excitations and is meaningful to the seismic design of SFTs, as well as other periodic long-span structures. Mirzapour et al. (2016) investigate the response of submerged floating tunnel with not only spatial variation of seismic ground motion, but also additional force of surrounding fluid on the tunnel due to seismic motion. The model design is a long 2000m span tunnel; the author shows the effects of 2D and 3D fluid field. The results show that the maximum deflection increase along the tunnel length, which is near the left support point. This paper studies the effects of the stiffness of tethers by changing the mooring line stiffness values of the tunnel and the influence of stiffness will occur at the natural frequencies of the SFT.

In Di Pilato et al. (2008), SFT was considered as a multi-supported structure associated with seismic waves. The research presented the significance of soil-structure interaction and suggested general considerations related to dynamic behavior. Cheng (2014) analyzed the bidirectional seismic effects of the fluid-structure interaction of the submerged floating tunnel in a broken fault zone. By using ADINA, which is the finite element analysis software, the author investigates the effects of the both horizontal and vertical seismic motion, and the displacement movement and stress of tunnel at the three points. The results show that the horizontal motion of the tunnel is bigger than vertical motion, meaning that horizontal motion is significant responses of tunnels. Furthermore,

the tunnel vault point is the weakest part in the seismic condition, because the maximum acceleration occurs at tunnel vault point.

Lee et al. (2016) performed a numerical study of the effects of hydrodynamic pressure due to earthquake on the seismic response of SFT. They examines the effects of submerged floating tunnel system with two dimensional seismic motions using four components: fluid compressibility, the seawater depth, tunnel location in the water, and energy absorption of the tunnel. The hydrodynamic pressure is used to consider interaction of fluid and structure. It demonstrates that the horizontal seismic motion does not significantly affect the tunnel motion based on four components of vertical seismic motion. A low frequency mooring line force dominates, so the low frequency roll and sway motions are remarkable factors under seismic response of the tunnel. These effects must be considered for accurate and economical seismic designs of SFT systems. That is, the focus was on the effect of earthquake-induced acoustic wave pressure (due to compressibility) on the elastic structure induced by seismic motion. However, in my research, I focused on the transimissibility of ground motion to the structural respoonse through mooring line with assuming of rigid body structure and incompressible fluid under seismic ground conditions. Most studies investigated the dynamic responses of SFTs based on one type of mooring line arrangement. In addition, they mostly focused on a single environmental condition such as an earthquake and a wave load.

CHAPTER III

METHODOLOGY

3.1 General equation of motion for submerged body

3.1.1 Linear wave theory

This numerical analysis was designed to investigate the dynamic behaviors of submerged floating tunnels (SFTs) to certain ocean conditions. For the hydrodynamic load, a Morison equation was used. The general Morison equation has two force components: inertia force and drag force, and it divided by two siuation, fixed body and moving body.

The Morison equation for a fixed body is;

$$F = \rho C_M \forall \ddot{\eta} + \frac{1}{2}\rho C_D A \dot{\eta}|\ddot{\eta}| \tag{3.1}$$

In Equation (3.1), ρ is the seawater density, C_M *(= 1+*C_A*)* is the inertia coefficient, C_D is the drag coefficient, $\forall$ is the volume of body, A is the cross sectional area perpendicular to the wave propagation, and $\dot{\eta}$ is the wave velocity and $\ddot{\eta}$ is the wave acceleration.

The Morison equation which is modified for calculating moving body while same principle is applied in OrcaFelx (2015). In OrcaFlex (2015), the properties such as mass, weight, and buoyancy are considered as lumped mass element to simplifies the mathematical formulation. Generally, the hydrodynamic load was based on Morison equation and the hydrodynamic load was applied at the center of the tunnel cylinder structure if the added mass and damping were also considered to be lumped.

The extended formulation of the Morison's equation is;

$$F = C_M \rho \frac{\pi D^2}{4} \ddot{\eta} - C_A \rho \frac{\pi D^2}{4} \ddot{x} + \frac{1}{2} \rho C_D D |\dot{\eta} - \dot{x}| (\dot{\eta} - \dot{x}) \quad (3.2)$$

The following symbols $\ddot{x}$ and $\dot{x}$ are the acceleration and velocity of the structure, respectively. D is the diameter of the structure, C_A is the added mass coefficient.

In this study, the wave loads on the SFT is compute by means of the Morison equation. The complete second order wave forces are not considered. In addition, the simulation of seismic excitation is done by changing the anchor point of mooring lines at each time step.

3.1.2 Equation of motion under seismic excitation

For analyzing SFT model with multi supported mooring structure under seismic excitation, the proposed governing equation by dynamic of structures (Chopra, 2007) is:

$$(M + M_{Add}(\infty))\ddot{x}(\mathrm{t}) + (K_{hydro})x(t) = F_{wave} + F_{drag} + F_{mooring} \quad (3.3)$$

where M is mass, M_{Add} is added mass, K_{hydro} is hydrostatic restoring coefficient, F_{wave} is wave exciting force, and $F_{mooring}$ is mooring-induced force. $\ddot{x}$ and x are acceleration, velocity, and displacement of the structure, respectively. The applied external force at the ground is not considered, because the motions of structure is major point of this research.

3.2 Information of tool

The modeling and numerical analysis of a Submerged Floating Tunnel (SFT) and mooring line under diverse conditions such as linear wave, nonlinear wave, and seismic situation effect is performed to investigate the coupled dynamic response. There are two different types of mooring line, vertical and inclined, and these are studied to figure out

the tunnel displacement motions and mooring line tension with the three conditions; regular wave, nonlinear wave, and seismic wave. For the seismic wave condition, external loading motion was allowed for multiple-support seismic excitation by using real time series displacement values, adding non-linear hydrodynamic loads as wave for tunnel and mooring line.

For this study, two different software was used to analyze model. First simulation is OrcaFlex (2015), a commercial software widely used for the dynamic analysis of offshore system such as floating platforms and all types of moorings under wave load and externally imposed motions in the offshore industry. A second tool is CHARM3D(Coupled Hull And Riser Mooring 3D) (Kim, 2005). It is the finite element program and developed by Texas A&M University for coupled dynamic analysis of mooring system. The details mathematical formulation of both software are to be presented in the following section.

3.2.1 CHARM3D

The program is frequency domain and time domain simulation for coupled dynamic analysis of offshore structure such as platform and mooring line based on a finite element method in cluding first and second order depend on frequency effects. For time domain, the various factor of nonlinearities such as mooring line drag force, column drag force, large motions of the platform, mooring line geometric nonlinearity are able to be included. For frequency domain, the structure is assumed to experience small movement around the mean position, because of this linear anlysis can be used. For mooring system,

the elastic rod model can be used for simulating based on the single global coordinate system of finite element formulation. This theory is proposed by Garrett (1982) and it explained that the effects of buoyancy and hydronamic load due to wave and current, and the effects of gravity, line mass.

To determine the element motions, the center position of rod is applied. The coordinate system is defined with position vector *r(s,t)* at arc length s and time t. The equation of motion is followed:

$$-(EIr'')'' + (\lambda r')' + q = \rho_r r$$

$$r' \cdot r' = \left(1 + \frac{T}{EA_I}\right)^2 \approx 1 + 2\frac{\lambda}{EA_I} \tag{3.4}$$

In Equation (3.4), it is presented by including bending stiffness, axial stiffness, hydrostatic loads, hydrodynamic loads. *E:* Young's modulus of the rod, *I:* Inertia moment of cross section, q: distributed load, ρ_r: rod density, T: axial tension, A_I: cross sectional area and λ: Lagrangian multiplier. Dots serve as derivatives according to time and apostrophes serve as position derivatives.

Modified distributed load include hydrostatics and hydrodynamic loading in shown as Equation (3.5) where w: rod weight by unit length, F^s: hydrostatic force per unit length and F^d: hydrodynamic force per unit length.

$$q = w + F^s + F^d \tag{3.5}$$

In addition, the hydrodynamic loads include buoyancy force per unit length, B, and hydrostatic pressure, P, at point r on the rod. The equation is followed;

$$F^s = B - (PA_I r')' \tag{3.6}$$

As aboved mention, the modified Morison equation with respect to relative motion is used to determine the hydrodynamic force. The particular form is followed in Equation (3.7) where C_A, C_M and C_D are added mass, inertia and drag coefficients, r^n and r^n are rod member velocity and acceleration normal to rod centerline, ρ is water density, A_D is area of the unit length rod projected to the plane normal to the rod centerline, V^n and V^n are velocity and acceleration of the water normal to the rod centerline because of the incident wave and current.

$$\begin{aligned} F^d &= -C_A \rho A_I r^n + C_M \rho A_I V^n + C_D \rho A_D \left|V^n - r^n\right| (V^n - r^n) \\ C_M &= C_A + 1 \end{aligned} \tag{3.7}$$

The final equation form of structure motion for the rod is shown in Equation (3.8), by combining Equations. (3.4), (3.5) and (3.6).

$$mr + C_A \rho A_I r^n + (EIr'')'' - (\lambda r')' = w + F^d$$

$$\begin{aligned} &\textit{where} \\ &m = \textit{mass per unit length} \\ &\lambda = T - EI\kappa^2 \\ &\kappa = \textit{local curvature} \\ &w = w + B : \textit{wet weight of the rod} \\ &T = T + P : \textit{effective tension in the rod} \\ &F^d = C_M \rho A_I V^n + C_D \rho A_D \left|V^n - r^n\right| (V^n - r^n) \end{aligned} \tag{3.8}$$

The forces which is act on the tuennl and displacements can be calculate base on the values of r and λ. In this research, the value of C_D and C_M are fixed based on standard values of cylinders under wave conditions.

3.2.2 OrcaFlex

After the static analysis generates the starting position of the motions, the dynamic analysis continues the simulation in time domain. Through OrcaFlex, lines and 3 or 6 degree of buoys can be examined to discretize the system. For this research, mooring lines and 3 degree of freedom buoys are used to discretized SFT model in OrcaFlex (2015). The weight, buoyancy, drag force, added mass and reactions was effected through 3D buoys. The lines are modelled as massless spring segments by using nodes to connect each other. Also, it performs the axial, torsional and bending properties of the segment. To connect between tunnel of SFT and mooring lines, the three degree of freedom buoys are employed. This buoys are performed as connection nodes, so the hydrodynamic contribution is neglected in this study.

Based on the lumped mass theory in this case, the final equation of motion is influenced by effects of tension, external pressure by hydrodynamic force, internal pressure for cylindrical pipe, bending and shear force. Such case excludes the effects of torsion and internal pressure.

In order to implement dynamic integration of the system, the equation of motion is given in Equation (3.9). For this calculation, explicit integration scheme was used with

a constant time step. With an appropriate time step, this method allows efficient simulations (Orcina, 2015)

$$M(p,a) = F(p,v,t) - C(p,v) - K(p) \tag{3.9}$$

Where, *M(p,a)* is the inertia load, *F(p,v,t)* is the external load, *C(p,v)* is the element damping load, and *K(p)* is the stiffness load. *p,v,a* and *t* are the position, velocity, acceleration and simulation time step, respectively. The Equation (3.9) is applied to each free body and line node. The function of *F(p,v,t)* considers the force F^d *(t)* as well as buoyancy and gravity force.

As mentioned before Morison equation, it includes C_M, added mass coefficient, and C_D, drag coefficient. In OrcaFlex, the velocity normal to the direction of line element and flow field gives C_D a changing value while C_M remains as a constant number. In this simulations, constant valued of the inercia coefficient, C_M, is 2 (C_A=1), and it was used for both numerical simulations since the SFT is circular cylinder. For drag coefficient, C_D, DeCrew (2010) formulation was used in OrcaFlex, despite constant valued of drag coefficient, 1.2, was used in CHARM3D. The variation in C_D values for submerged structure is explained through a study done by DeCew (2010). DeCew (2010) proposed the formulas by considering from laminar flow to turbulent in order to reduction of drag at high *Re* values. The formulation is presented in Equation (3.10).

$$C_D = \begin{cases} \dfrac{8\pi}{Res}(1-0.87s^{-2}), & 0 < Re < 1 \\ 1.45 + 8.55Re^{-0.9}, & 1 < Re \le 30 \\ 1.1 + 4Re^{-0.5}, & 30 < Re \le 2.33x10^5 \\ -3.41x10^{-6}(Re - 5.78x10^5), & 2.33x10^5 < Re \le 4.92x10^5 \\ 0.401(1 - e^{-Re/5.99x10^5}), & 4.92x10^5 < Re \le 10^7 \\ s = -0.077215655 + ln(8/Re) & \end{cases} \tag{3.10}$$

By using this formulas, hydrodynamic loads and mooring lines of SFT structure can be calculated accurately.

In case of OF, the Wheeler stretching method is used for the realistic prediction of velocity and acceleration of a fluid particle in Airy wave theory while CHARM3D uses original equations in Airy wave theory (Wheeler, 1969). The general horizontal particle velocity in Airy wave theory is

$$u(x,z,t) = \omega\eta_a \frac{cosh\,(k(z+h))}{sinh\,(kh)} sin\,(\omega t - kx) \tag{3.11}$$

where ω is angular frequency, η_a is wave amplitude, k is wave number, and h is water depth. The term, $cosh(k(z+h))/sinh(kh)$, leads to exponential decay of velocity as z is less than zero (free surface) and amplification of velocity as z is greater than zero. In Wheeler stretching method, better estimation of velocity and acceleration can be made by replacing the vertical coordinate, z, with z' as follows:

$$\mathrm{z'(x,t)} = \frac{h(h+z)}{h+\eta(x,t)} - h \tag{3.12}$$

where η is wave elevation. For two different simulation programs, the Morison forces are estimated at the instantaneous positions of SFT at each time step. For mooring line analysis, OrcaFlex uses massless springs, which represent axial, bending, and torsional behaviors, and springs are connected to nodes where mass, weight, buoyancy, and other properties are lumped into the nodes (Orcina, 2015). Mooring line analysis of CHARM3D is used the line dynamics of inextensible slender rods which is based on the high-order finite element method (FEM). The effect of gravity force, hydrodynamic loads, and ground boundary conditions are included for the line dynamics (Garrett, 1982). For making models this case, SFT was modelled based on the model scale conditions. In both tools, regular waves based on wave height and wave period by using linear Airy wave, and JONSWAP spectrum is applied for random waves. Such procedure is implemented to avoid the inconsistency of data when attaining tension and displacements information.

CHAPTER IV

DESCRIPTION OF CONDITIONS*

4.1 Model description

The characteristic of SFT is 98m of a length, 23m of a diameter, and 0.275m of thickness. The mooring diameter is 0.12m, density is 0.8ton/m^3, and elastic modulus is 197.0 Gpa. And BWR (buoyancy-weight ratio) is 2.6. SFT model is located in 41.5m from free surface and water depth is 80m. For numerical simulation, the model of SFT is used 1:100 scale factor to validate model design. SFT model design is proposed by Oh et al. (2013) and comparison between numerical analysis through modeling and experimental results under regular wave conditions have been conducted by Oh et al. (2013) and Cifuentes et al. (2015). The basic configuration of SFT with vertical and inclined mooring line is given in Figure 4.1.

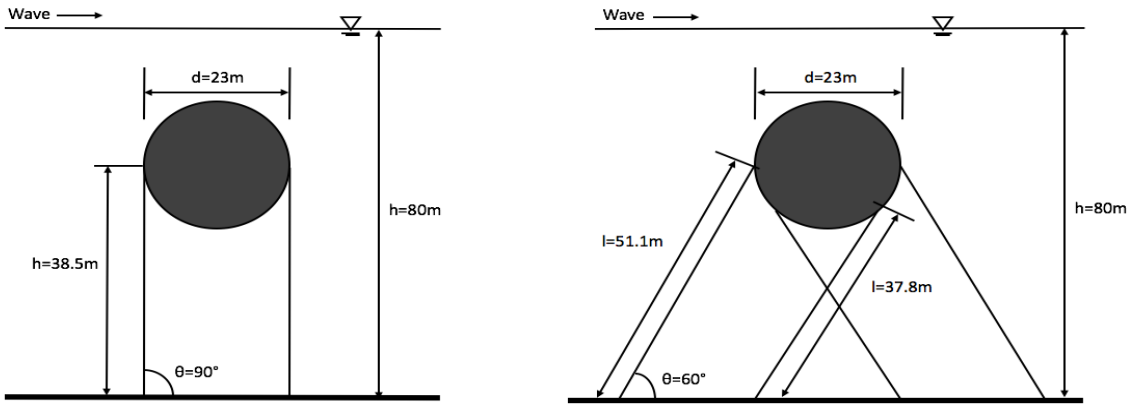

Figure 4.1 basic concept of SFT

* All figures in this chapter are reprinted with permission from "Dynamic response analysis of submerged floating tunnels by wave and seismic excitation" by J.Y. Lee, C.K. Jin, and M.H. Kim 2017. Ocean System Engineering, Vol. 7, No.1, Copyright by Techno Press.

4.2 Environmental conditions

In this study, three environmental conditions: regular wave, irregular wave and seismic excitation, are applied to SFT models for analyzing dynamic motion of SFT and mooring line tension. As above-mentioned, the experimental results under regular wave conditions were given by Oh et al. (2013). Numerical simulation, which is conducted by Cifuentes et al. (2015), compared with experimental results to validate the model design. This experimental results also are used to demonstrate for our numerical model under regular wave conditions. Through this validating step under regular wave conditions, two types of SFT are investigated to identify the accuracy of numerical design for next following research.

4.2.1 Regular wave

For regular hydrodynamic loads, Airy wave theory is use and applied on both simulation. The conditions of regular wave are given in Table 4.1.

Table 4.1 Regular wave conditions

Wave Period	*Wave Height (m)*	*Wave Steepness (s)*
6.5	0.85	0.013
	1.75	0.027
	2.65	0.040
	3.50	0.053
8.0	1.30	0.013
	2.70	0.027
	4.00	0.040
	5.30	0.053
10.0	2.00	0.013
	4.10	0.027
	6.20	0.040
	8.20	0.053
13.0	3.20	0.013
	6.50	0.027
	9.80	0.040
	13.00	0.053

4.2.2 Irregular wave

In OrcaFelx, four types of random wave conditions are offered; JONSWAP, ISSC, Ochi-Hubble and Torsethaugen (Orcina, 2015). For this study, JONSWAP spectrum with γ of 3.3 is used to provide the irregular wave conditions with responded to H_s, T_p: wave height and spectral peak period, repectively. Superposed 100 wave components were use to generate irregular wave. The tool use time history by synthesizing of user-determined values about wave conditions (Orcina, 2015). For each wave case, 3 hours is carried out in this simulation. The wave elevation time series which are gained from CHARM3D are employed at OrcaFlex to demonstrate the precision and motion results of two numerical simulation (OrcaFlex and CHARM3D) especially under extreme wave condition. The irregular wave conditions are given in Table 4.2.

Table 4.2 Irregular wave conditions

Case#	Significant Wave height (m)	Peak period (s)
1	0.09	2.0
2	0.67	4.8
3	1.40	6.5
4	2.44	8.1
5	3.66	9.7
6	5.49	11.3
7	9.14	13.6
8	15.24	17.0

4.2.3 Seismic excitation

Displacement-time history is important value to analyze seismic motion. The both direction real seismic time history data such as horizontal(X-direction) displacement and vertical(Z-direction) displacement is used to estimate the motion of SFT and mooring line tension by comparing between vertical mooring line condition and inclined mooring line condition. To validate the seismic behavior of SFTs, the tendency of two different types of SFTs were initially analyzed due to a linear seismic motions. The earthquake-generated linear ground motion were assumed and applied. The assume conditions are that the seismic frequency is 0.5Hz, 0.75Hz, 1.0Hz, and 1.25Hz, and amplitude is 0.1m, 0.2m, and 0.01m. After analyzing the numerical simulation of those linear seismic condtions, and then the real time seismic displacement data is applied to ground motion at anchor points. For real seismic condition, four real earthquake events from earthquake in California and Hawaii were selected and employed to derive the reponses of SFTs subjected to seismic motion. The characteristics of the selected real seismic conditions are shown as Table 4.3,

and the time history of the both horizontal and vertical displacement are illustrated in Figures 4.2 and 4.4. Also, the corresponding spectrums of surge motion with both direction are shown as Figures 4.3 and 4.5. Horizontal and vertical ground seismic motions are used at both linear seismic motions and real seismic motions.

Table 4.3 Characteristics of earthquake conditions

Earthquake	Magnitude	Horizontal Peak motion (cm)	Vertical Peak motion (cm)
Green Valley – California	3.90	-0.03	- 0.0107
Honomu – Hawaii	4.90	0.06	-0.00347
Offshore Northern – California	5.40	0.16	0.0743
WNW of Ferndale – California	6.80	2.20	- 1.7

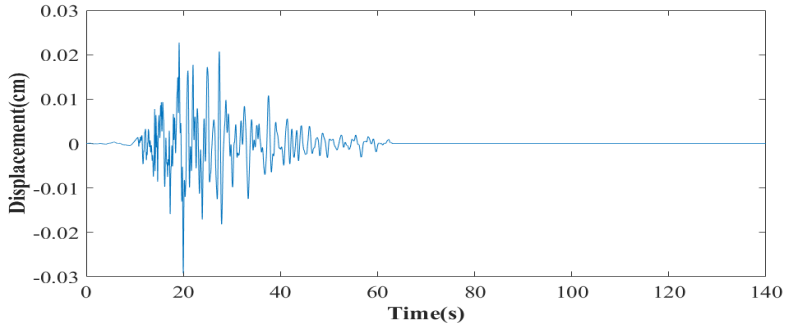

(a) Green Valley, California (Magnitude = 3.9)

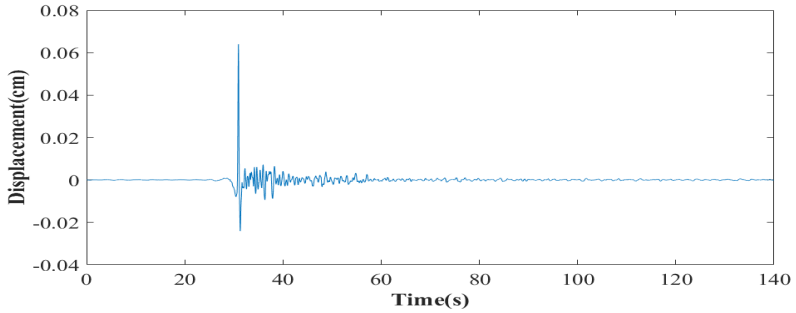

(b) Honomu, Hawaii (Magnitude = 4.9)

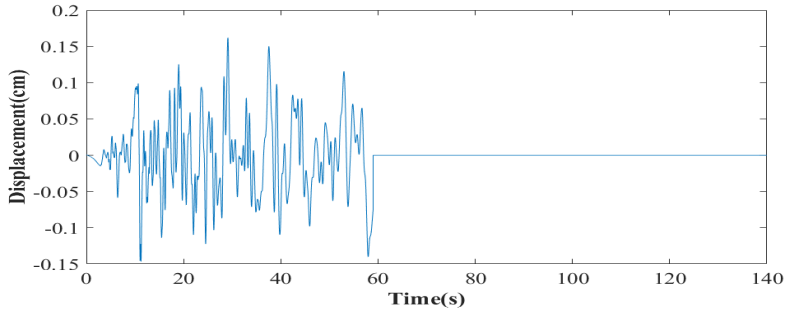

(c) Offshore Northern, California (Magnitude = 5.4)

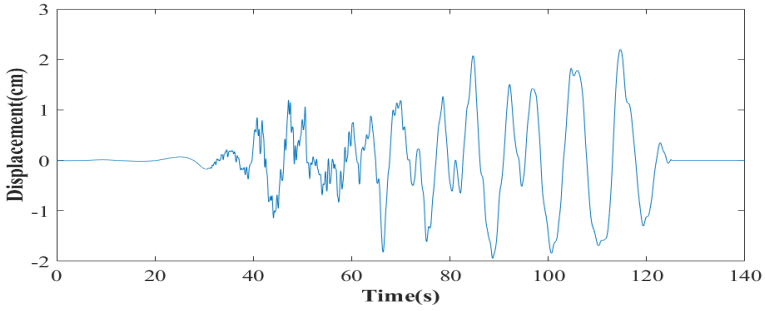

(d) WNW of Ferndale, California (Magnitude = 6.8)

Figure 4.2 Selected horizontal displacement motion time history: duration time 140 sec.

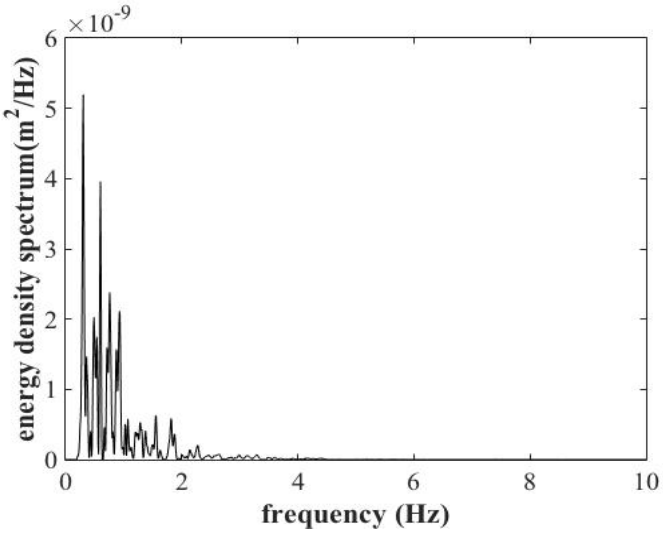

(a) Green Valley, California (Magnitude = 3.9)

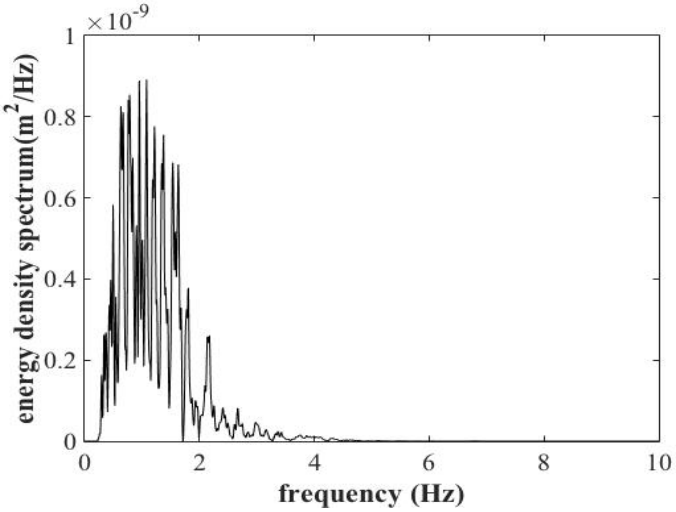

(b) Honomu, Hawaii (Magnitude = 4.9)

Figure 4.3 Energy density spectrum of real horizontal seismic motions.

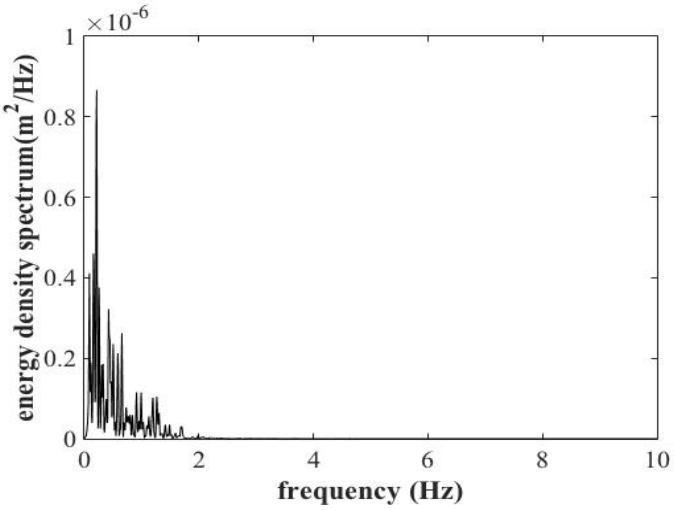

(c) Offshore Northern, California (Magnitude = 5.4)

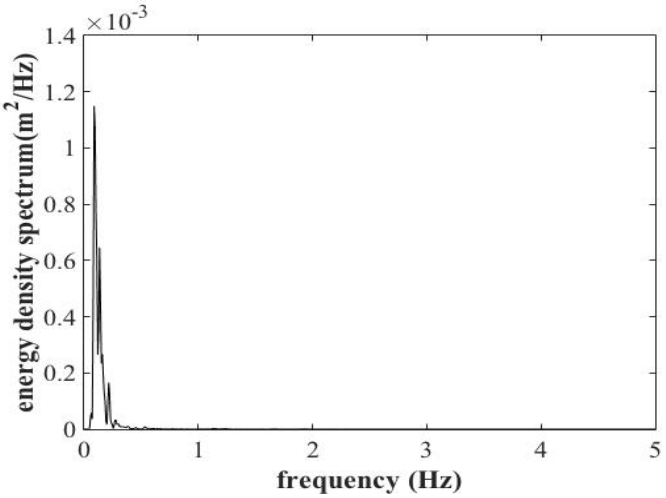

(d) WNW of Ferndale, California (Magnitude = 6.8)

Figure 4.3 continued

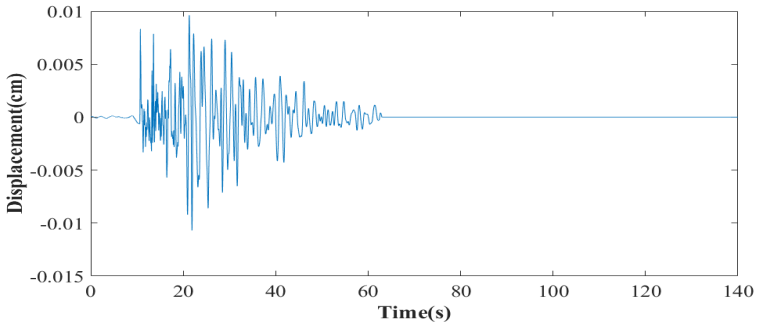

(a) Green Valley, California (Magnitude = 3.9)

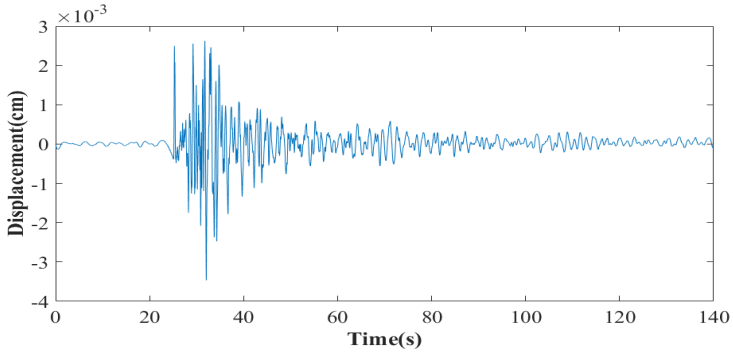

(b) Honomu, Hawaii (Magnitude = 4.9)

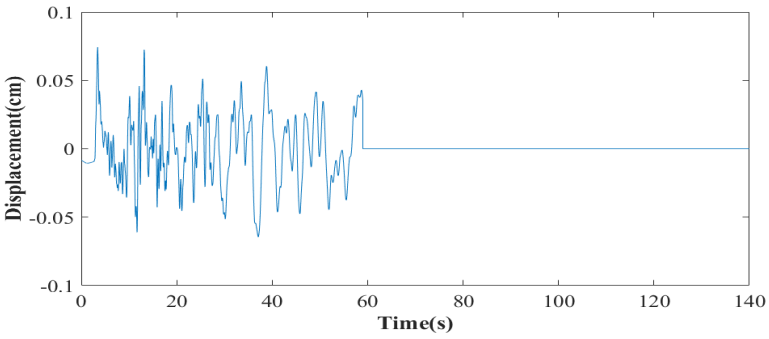

(c) Offshore Northern, California (Magnitude = 5.4)

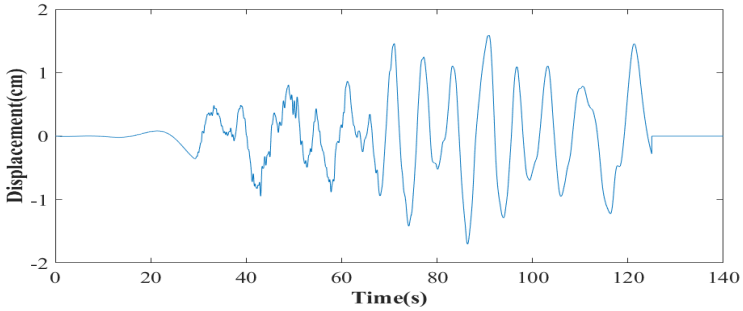

(d) WNW of Ferndale, California (Magnitude = 6.8)

Figure 4.4 Selected vertical displacement motion time history: duration time 140 Sec.

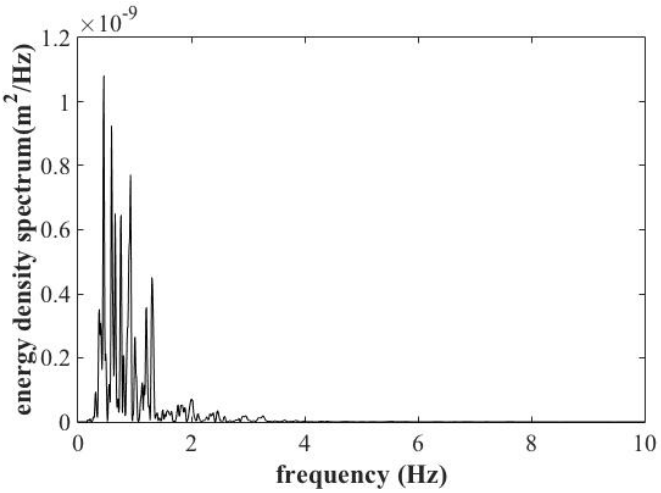

(a) Green Valley, California (Magnitude = 3.9)

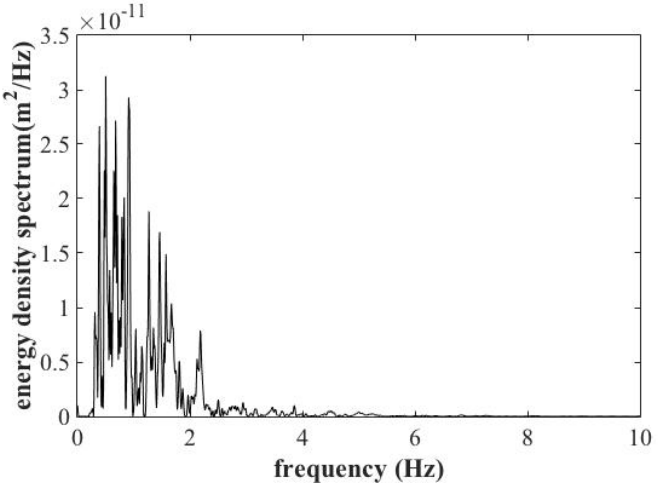

(b) Honomu, Hawaii (Magnitude = 4.9)

Figure 4.5 Energy density spectrum of real horizontal seismic motions.

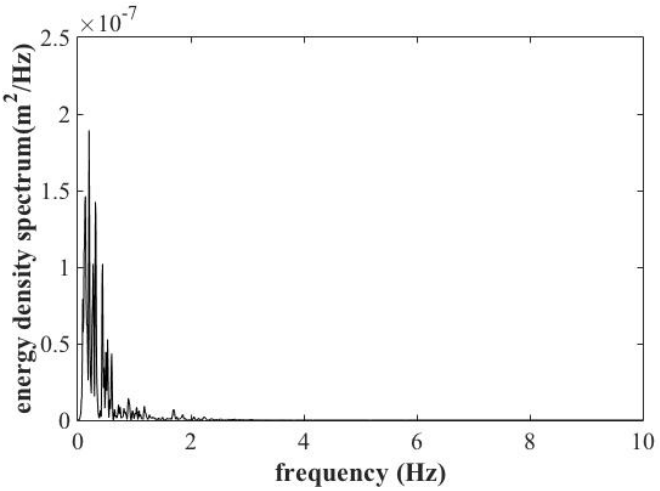

(c) Offshore Northern, California (Magnitude = 5.4)

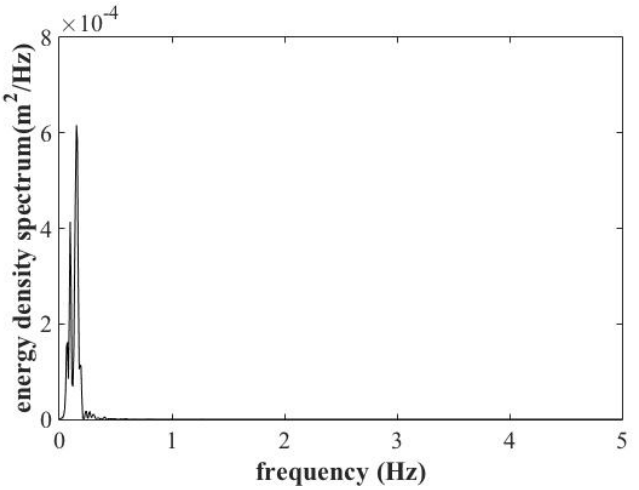

(d) WNW of Ferndale, California (Magnitude = 6.8)

Figure 4.5 continued

CHAPTER V

RESULTS OF NUMERICAL SIMULATION*

In this chapter, the dynamic responses of the model SFTs are described in order to examine the effects of their hydrodynamic and seismic loads. First, the SFT model designs were validated by comparing the results with experimental data under regular wave conditions. Next, based on the model SFTs, their dynamic behaviors were examined by comparing the results produced by two numerical analysis software packages: OrcaFlex and CHARM3D. Thereafter, the displacement motion responses were analyzed, including realtime seismic ground motion with both horizontal and vertical components. In this step, the SFTs' dynamic motion trends were evaluated according to the models' design components.

5.1 Results under regular wave conditions: Validation of the numerical models

As mentioned above, a numerical analysis under regular wave conditions was performed by Cifuentes et al. (2015), and an experiment was conducted by KIOST (Oh et al., 2013). The numerical simulation was based on the same conditions as the SFT models' designs; this was proposed before this research was conducted, as a means of validating the model designs under the same regular wave conditions. The models were based on a

* All figures in this chapter are reprinted with permission from "Dynamic response analysis of submerged floating tunnels by wave and seismic excitation" by J.Y. Lee, C.K. Jin, and M.H. Kim 2017. Ocean System Engineering, Vol. 7, No.1, Copyright by Techno Press.

scale factor of 1:100. In real scale, the tunnel portions were 98m in length and 23m in width. The mooring lines were 0.12m in diameter; there were two angles: 90^{o} for the vertical tethers and 60^{o} for the inclined tethers. The buoyancy of weight ratios (BWR) of the tunnels were focused at a low 2.6.

The complete dynamic behavior SFT simulation model is illustrated in Figure 5.1, below. The left portion is the vertically moored SFT, which was oriented to be perpendicular to the seabed, and the right portion is the incline moored SFT, which was oriented at a 60^{o} angle from the flat bottom seabed. In the modeling process, an Airy wave was used for regular wave conditions, which took the form of a wave traveling perpendicular to the tunnel's axial direction. As discussed above, a Morison equation was also used, and the drag coefficient of the submerged floating tunnel, C_D, as proposed by DeCew, was applied in OrcaFlex.

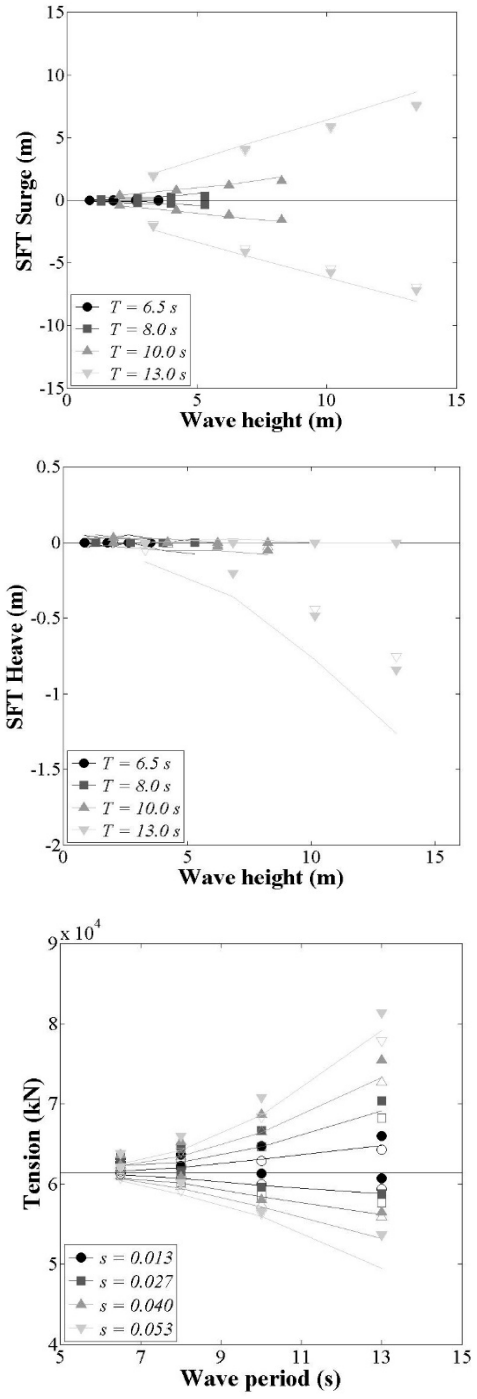

Figure 5.1 Numerical results for the (a) surge, (b) heave, and (c) tension of the vertical mooring lines for the experiment, CHARM3D, and OrcaFlex, as a function of wave height and period. (Solid lines represent the experiment, open markers denote OrcaFlex, and solid markers indicate CHARM3D.)

Figure 5.1 illustrates the dynamic responses of the tunnel and mooring line tension in the vertically moored SFT under regular wave conditions. The characteristics of this wave condition included: a wave period from 6.5s to 13.0s, maximum height from 0.8m to 13.0m, constant BWR of 2.6, and water depth of 80m. With regards to predicting the wave kinematics, the Wheeler stretching method was used for the hydrodynamic elevation time series in OrcaFlex. Then, the surge, heave, motion, and mooring line tension results from OrcaFlex and CHARM3D were compared, along with the experimental results found in the previous research. As shown in Figure 5.1, the dynamic characteristics of the numerical models were in excellent agreement with the experimental results, thus validating the test model under regular wave conditions. The wave and surge of the SFT presented a constant phase. The surge motion of the SFT was precisely proportional to the wave height and period. In the two small-wave conditions, the wave periods were 6.5s and 8.0s. The surge motion was not significant because the mooring lines did not restrict the horizontal motion. Despite the increase in surge motion and along with the upsurges in wave height and period that occurred in response to the other two wave conditions, the wave periods were 10.0s and 13.0s.

The heave motion was small when the wave height and period were small, and the negative heave motion was dominant in large wave conditions with long waves and high amplitudes. This was because movement was restricted when the mooring line stretched along the upper side of the tunnel, but there was no restriction effect when the mooring line pushed below the origin point; this was attributable to the design of the structure relying on the buoyancy of the tunnel. Even though the effects of interactions between the

fluid and the structure exist in reality, only numerical calculations were considered in this study. It was assumed that the body's movement did not significantly influence the changing wave field traveling along the SFT. The difference was probably due to nonlinear inclinations associated with slack mooring, as well as wave deformation by the SFTs in response to incident and radiation waves, conditions that were also mentioned by Cifuentes et al. (2015). In this research, these conditions were not numerically analyzed.

The tension plot was represented with a single mooring line because the signals from the four mooring components in the vertical configuration were similar in all wave conditions. Maximum and minimum loads were not perfectly symmetrical for the initial pretension. In terms of numerical and experimental data, the trend was well captured, except in extreme wave conditions (at a wave period of 13s). When nonlinearities regarding wave dynamics arose, the resulting level of agreement between the sets of data was acceptable. That is to say, the design of the tool matched well with the experimental model. Consequently, this model was used to develop the next step, as discussed below.

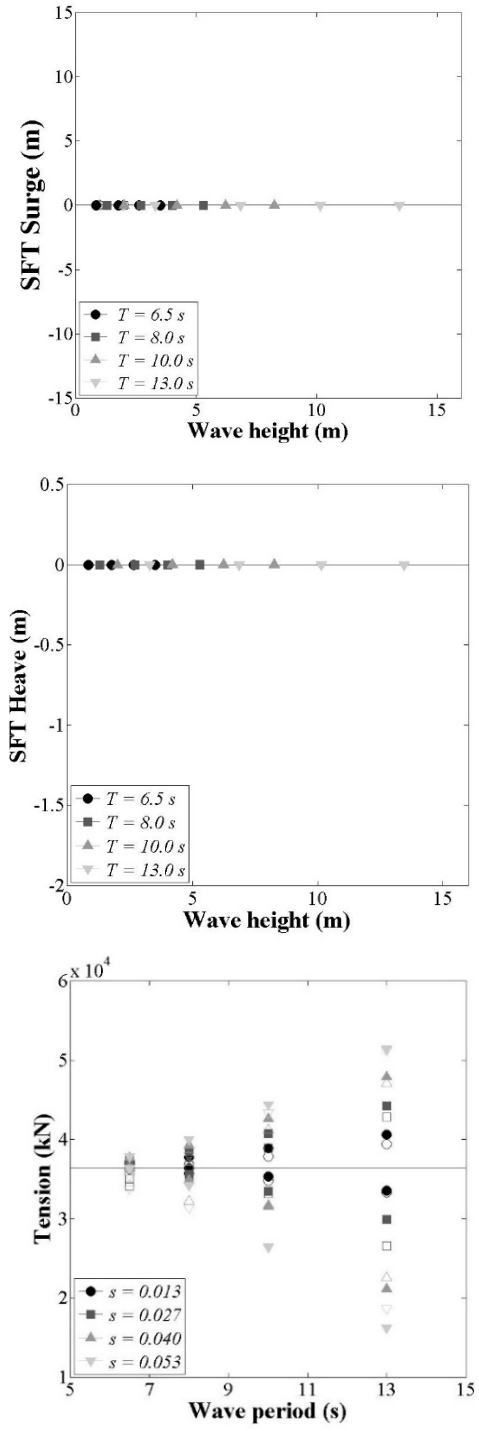

Figure 5.2 Numerical results for the (a) surge, (b) heave, and (c) tension of the inclined mooring lines for the experiment, CHARM3D, and OrcaFlex, as a function of wave height and period. (Solid lines represent the experiment, open markers denote OrcaFlex, and solid markers indicate CHARM3D.)

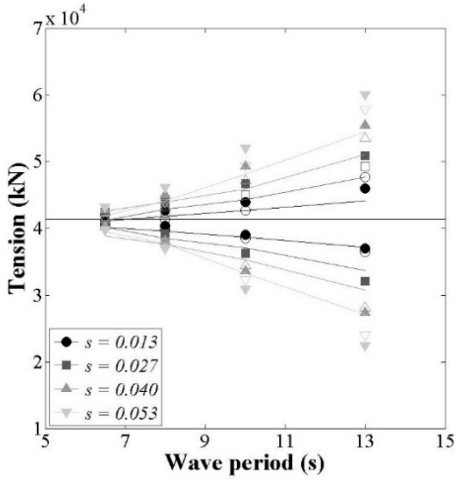

Figure 5.3 Comparison of inclined mooring line tensions from the experiment under regular wave conditions. (Solid lines represent the experiment, open markers denote OrcaFlex, and solid markers indicate CHARM3D.)

Figure 5.2 illustrates the surge, heave, and tension of the SFT with an inclined mooring line. Experimental data were not available for SFTs with inclined mooring lines. However, the results produced by OrcaFlex and CHARM3D were in reasonable agreement with one another. As discussed above, any variance is likely due to the drag coefficients and wave kinematics formulas employed. Additional verification of the inclined mooring line design was accomplished by comparing the results of the numerical simulations to those of the experimental data produced under similar conditions (case BWR=3.4). Figure 5.3 compares the inclined mooring line tensions. Generally, the numerical simulations were in accord with the experimental data.

As described above, eight mooring lines were used to connect the tunnel body on the incline moored SFT; four mooring lines are usually used with vertically moored SFTs. Due to this design concept, the effective mooring tension of a single line on a vertically moored SFT was higher than one on an SFT with inclined mooring (see Figures 5.1 and

5.2). However, the total effective mooring tension of an inclined mooring line was larger than that of a vertical mooring line. The tension force was proportional to the wave heights and periods, and followed the same trends as with vertical mooring. Unlike the conditions that result from vertical mooring, however, the surge and heave motions of the SFT were almost zero in terms of dynamic displacement responses. This is because the inclined mooring line effectively restricted the displacement of the SFT under regular wave conditions. It was clear that under regular wave conditions, the model design for an incline moored SFT would perform better than a vertically moored tunnel. Finally, the SFT model design was completely validated in this step, and thus was used for the subsequent steps in this research.

5.2 Results under irregular wave conditions

In this section, the SFT model is analyzed under irregular wave conditions, and the results from the OrcaFlex and CHARM3D numerical analyses are compared. As described above, SFT models with the same characteristics and under regular wave conditions were used. For irregular wave conditions (see Table 4.2), the JONSWAP spectrum with $\gamma = 3.3$ was employed in both OrcaFlex and CHARM3D. The SFT motions under irregular wave conditions are summarized in Table 5.1. The maximum surge motions and mooring tensions obtained from the two numerical simulations are illustrated in Figures 5.4 and 5.5. Figures 5.6 and 5.7 indicate the surges, heave motions, and mooring tensions of the numerical simulations of both SFT types at the extreme wave height of 15.24m and period of 17s. The tendencies of the surge and heave motions indicated by OrcaFlex were in excellent agreement with those provided by CHARM3D. There were no critical differences between the models produced by OrcaFlex and CHARM3D, except for the last extreme irregular wave condition: Case No. 8. However, this difference was not crucial as it was only approximately 10%.

Based on the surge motion results, the vertically moored SFT had a remarkably larger displacement than the SFT with inclined mooring, especially with regards to the maximum difference under extreme irregular wave conditions. The results indicate that an irregular wave height and period had a significant effect on the surge motion of the tunnel (See Figure 5.4 and Table 5.2). For example, the maximum surge motion of the vertically moored SFT was more than 25m, while its maximum heave motion was -9.9m under extreme wave conditions (Case 8, as shown in Figures 5.6 and 5.7). The results of both

numerical simulations were well in agreement and acceptable. As shown in Figure 5.5, both the mean and dynamic tensions of the SFT with vertical mooring were greater than those of the incline moored SFT. The maximum difference between the two types of SFT was approximately 38%; this was because the inclined mooring strategy (with eight mooring lines) was designed to reduce linear tunnel behavior related to hydrodynamic loads. Similar to regular wave conditions, the total effective tension of the SFT with inclined mooring was greater than that of the vertically moored SFT. Since both ends of the SFT were untethered, in extreme wave conditions the significant surge and heave responses of the vertically moored SFT were greatly inflated. In reality, this would be only an insignificant section of an extended SFT that would be tethered at both ends.

Table 5.1 Maximum and minimum values of the responses to irregular wave components

Case #	Significant wave height (m)	Peak period (s)	Surge (m)		Heave (m)		Tension (kN)	
			Min.	Max.	Min.	Max.	Min.	Max.
1	0.09	2.0	0.000	0.000	0.001	0.000	63925	63925
2	0.67	4.8	-0.006	0.006	0.001	0.000	63867	63989
3	1.40	6.5	-0.082	0.092	0.001	0.000	63392	64529
4	2.44	8.1	-0.454	0.464	-0.001	0.000	61870	66181
5	3.66	9.7	-1.401	1.528	-0.029	0.002	59780	69391
6	5.49	11.3	-4.075	4.658	-0.282	0.003	58297	73718
7	9.14	13.6	-12.559	15.070	-3.073	0.005	48396	89513
8	15.24	17.0	-21.626	27.950	-9.893	0.012	35514	126075

(a) SFT with vertical mooring

Table 5.1 continued

Case #	Significant wave height (m)	Peak period (s)	Surge (m)		Heave (m)		Tension (kN)	
			Min.	Max.	Min.	Max.	Min.	Max.
1	0.09	2.0	0.000	0.000	0.001	0.001	36248	36248
2	0.67	4.8	0.000	0.000	0.001	0.001	36169	36329
3	1.40	6.5	0.000	0.000	0.001	0.001	35497	37026
4	2.44	8.1	-0.001	0.001	0.001	0.001	33344	39344
5	3.66	9.7	-0.002	0.002	0.000	0.002	29881	43485
6	5.49	11.3	-0.003	0.003	0.000	0.002	25875	47554
7	9.14	13.6	-0.006	0.006	-0.001	0.002	18376	56196
8	15.24	17.0	-0.012	0.010	-0.002	0.003	4999	77628

(b) SFT with inclined mooring

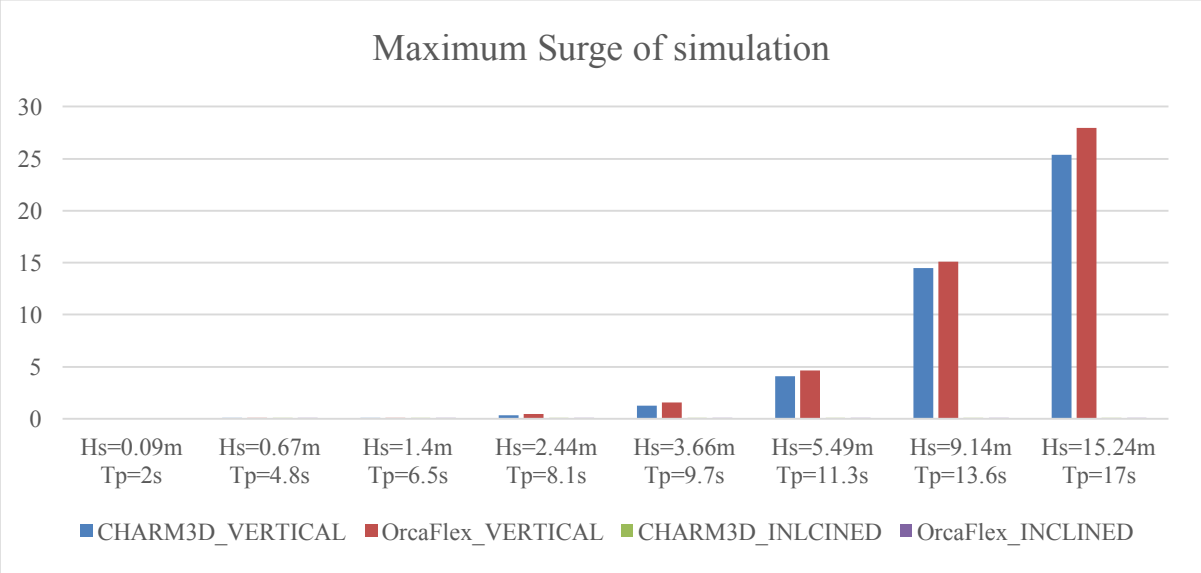

Figure 5.4 Numerical results in terms of wave height and period for the maximum surges of vertically and incline moored SFTs in CHARM3D and OrcaFlex.

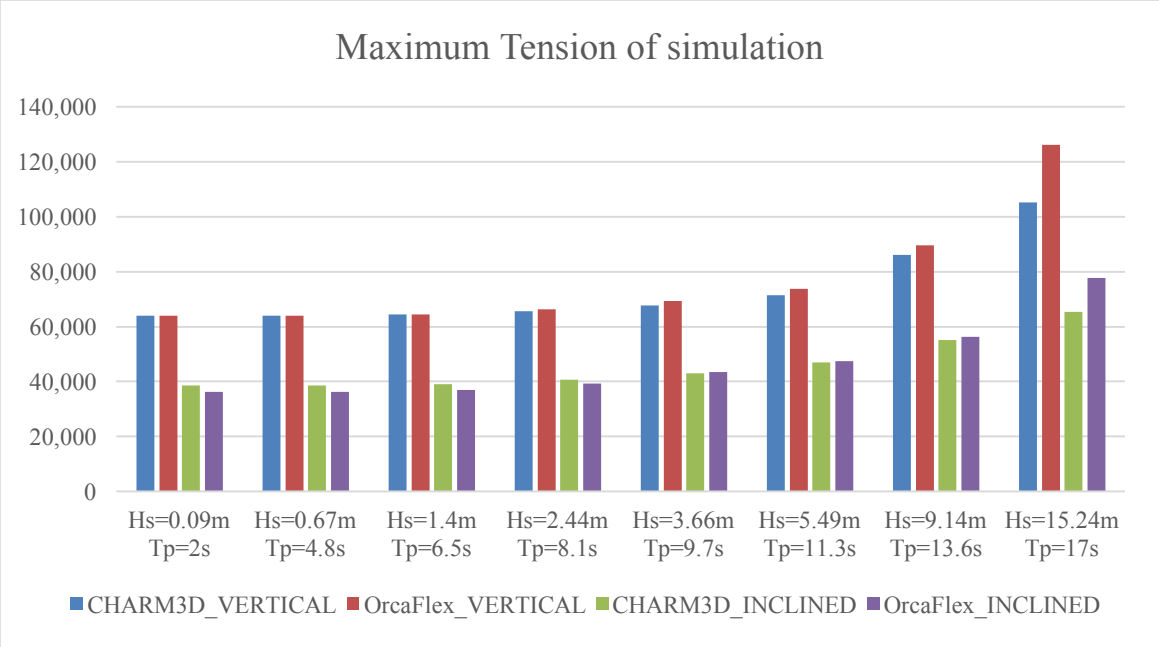

Figure 5.5 Numerical results in terms of wave height and period for the maximum tensions of vertically and incline moored SFTs in CHARM3D and OrcaFlex.

As described above, the wave elevation time series produced by CHARM3D was applied to the OrcaFlex time series to determine the accuracy of the motion described. The results shown in Figures 5.6 and 5.7 demonstrate that the simulations very closely coincided with one another for the two different types of SFT. Since the same input conditions were used for the incident irregular waves, the variances were most likely caused by the difference in drag coefficients (OrcaFlex uses the DeCew formula) and the Wheeler stretching method employed in OrcaFlex.

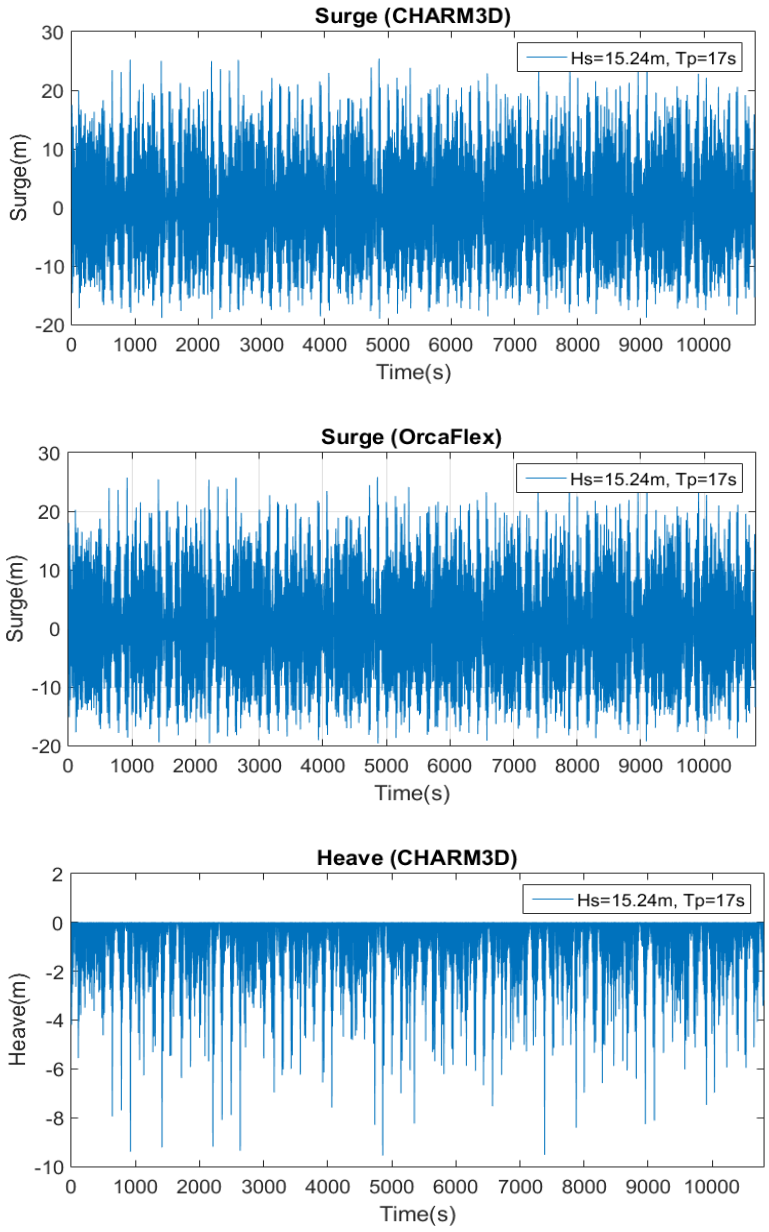

Figure 5.6 Numerical results for the (a) surge, (b) heave, and (c) tension of the vertically moored SFT in OrcaFlex and CHARM3D, under irregular wave conditions and with a wave height 15.24m and period of 17s.

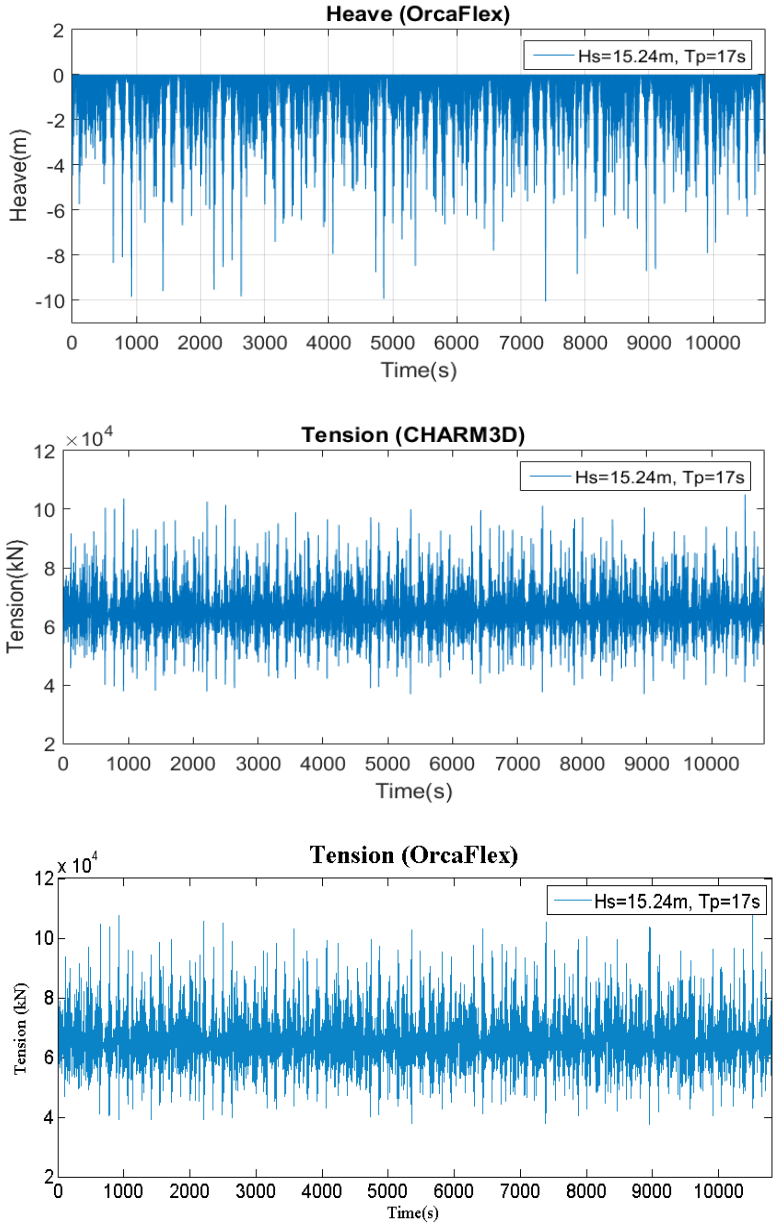

Figure 5.6 continued

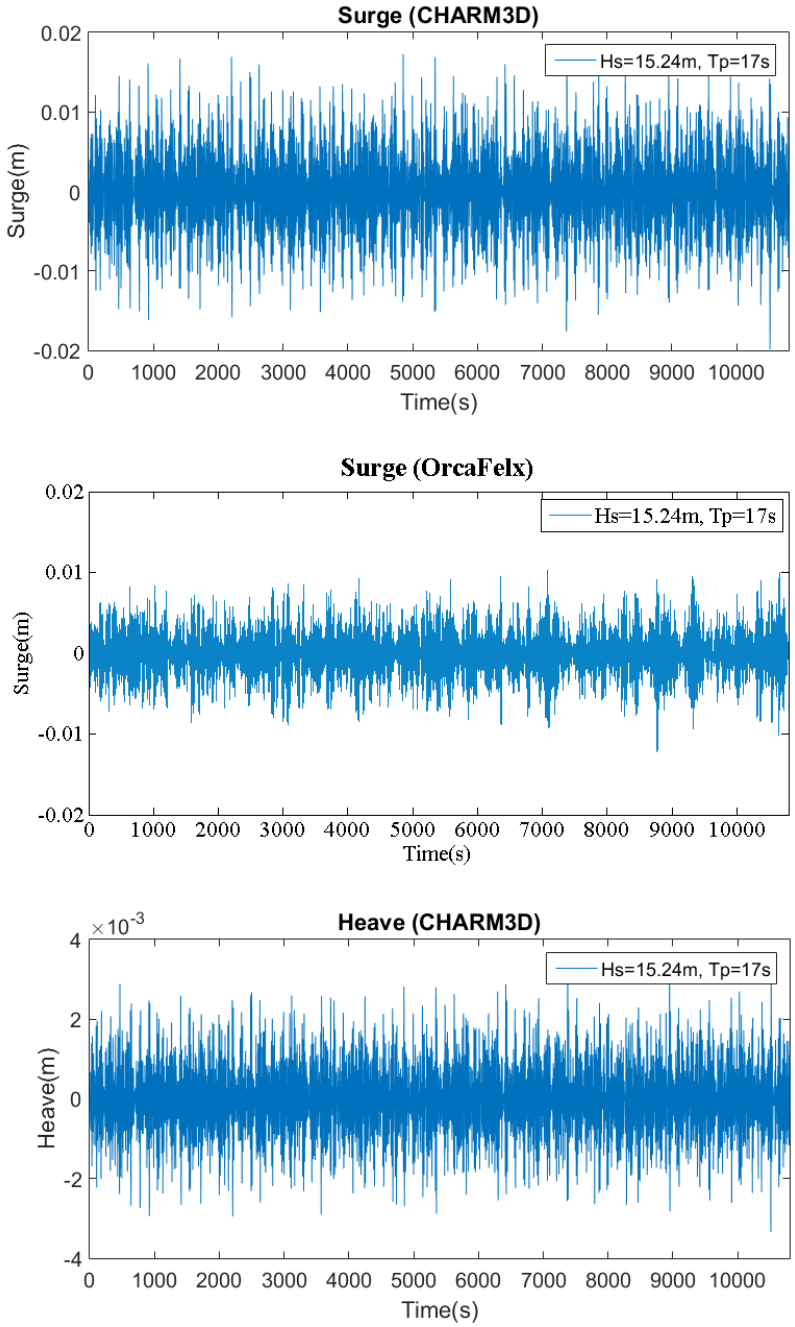

Figure 5.7 Numerical results for the (a) surge, (b) heave, and (c) tension of the incline moored SFT in OrcaFlex and CHARM3D, under irregular wave conditions and with a wave height of 15.24m and period of 17s.

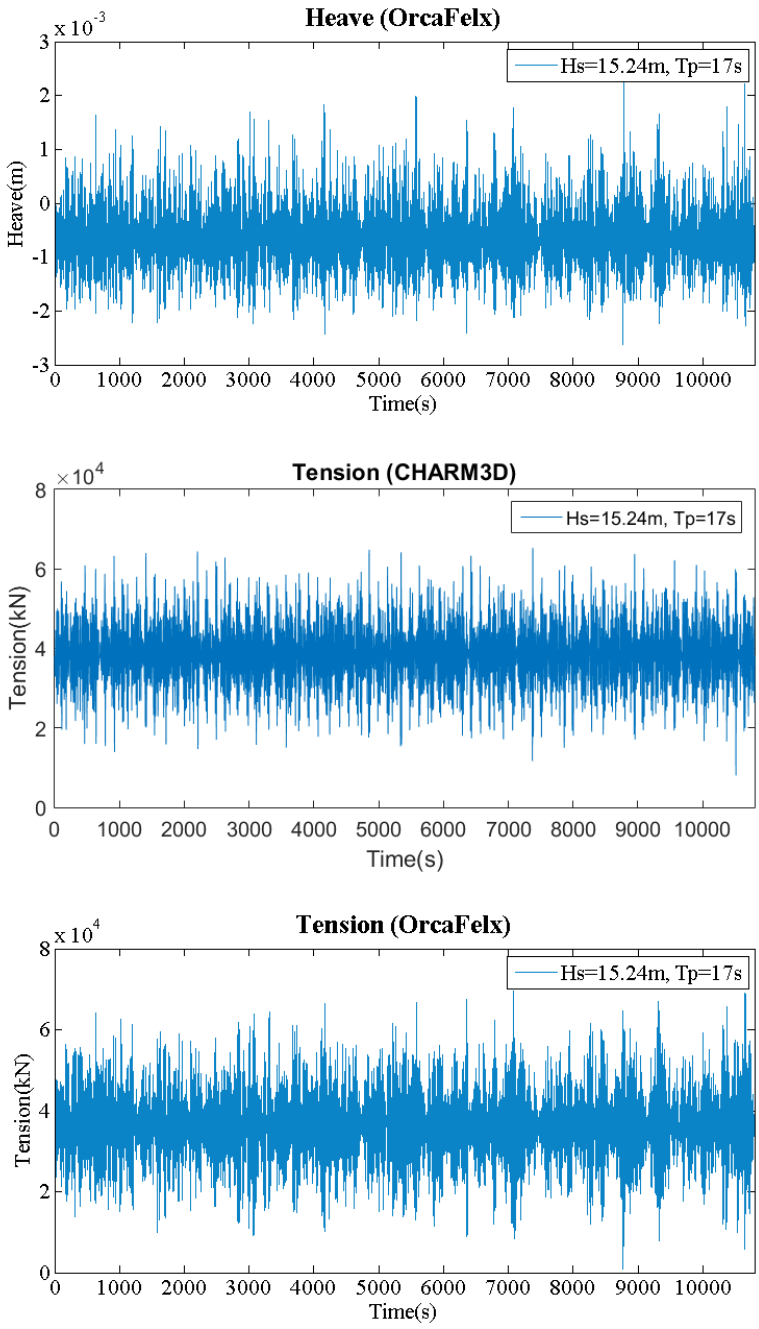

Figure 5.7 continued

5.3 Results from seismic conditions

5.3.1 Effects of linear seismic motion

The verified numerical models of the hydrodynamic load conditions were used to accurately examine the effects of seismic ground motion on SFTs. The seabed was regarded as a flat, frictionless, rigid foundation; the seismic motion traveled only in a parallel direction (i.e., the X- and Z-directions). One goal of this research was to conduct a dynamic motion analysis of the mooring lines and tunnels; thus, the seismic motion was the main focus and not a structural analysis. This is why the effects of acoustic wave pressure induced by earthquakes were not addressed, and instead this work analyzed the transmissibility of ground motion to the structure through the mooring lines (assuming a rigid structure and an incompressible fluid under seismic ground conditions). First, an analysis of the SFTs' dynamic movement was performed to evaluate the effects of linear seismic motion. The conditions had frequencies of 5Hz, 0.75Hz, 1.0Hz, and 1.25Hz, and amplitudes of 0.1m, 0.2m, and 0.01m. These values were chosen because they were determined to be representative of small and medium-scale earthquakes. The selected sinusoidal seismic activity traveled in a horizontal direction (the Z-direction) from the seabed and was applied to all of the anchored points by the same ground motion. Through the numerical analyses of these linear conditions, the tendency of the tunnel motion was investigated; the goal was to identify the accuracy of real seismic ground motion for the next step in this research.

Figures 5.8 and 5.9 illustrate the SFTs' seismic responses to the same frequency of motion, 0.5Hz, and the same amplitude, 0.01m, as determined by OrcaFlex and

CHARM3D. The results agreed well with one another. The surge motion of the SFT with inclined mooring gradually increased along with the 0.5% to 1.2% increase in the applied seismic motion. Conversely, the surge motion of the SFT with vertical mooring was not distinguishable from the of the incline moored SFT; it tended to follow the overall movement of the applied linear seismic motion. In this case, the heave motions of both mooring line systems were not dominant, as compared with the surge motions under horizontal ground activity. In other words, a surge motion significantly affected the motion of the structure only when seismic ground motion was employed.

Moreover, the maximum mooring tension of the vertically moored SFT increased with increasing seismic ground motion. The maximum difference in the tension values obtained by OrcaFlex and CHARM3D was about 11.48%. The dynamic tension of the vertically moored SFT tended to remain nearly constant in response to all linear seismic ground motions, whereas the dynamic tension of the incline moored SFT tended to increase with increasing linear seismic ground motion. The upper-most tension found in the incline moored SFT was greater than that of the vertically moored SFT when the amplitude was 0.2 m; the latter also showed no marked increase when the amplitude of the horizontal ground motion increased. From these results, it can be concluded that vertically moored SFTs should be employed to reduce dynamic surge motions when seismic conditions occur, even though the inclined mooring line tension was larger in response to applied horizontal seismic motion.

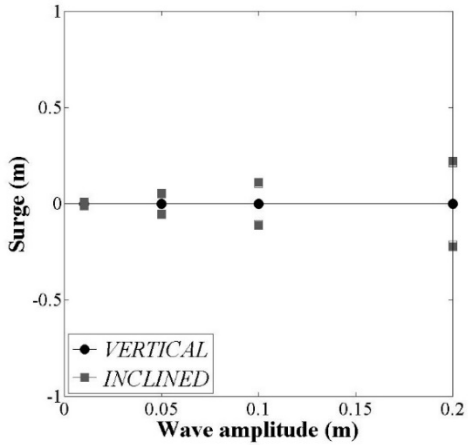

(a) Surge (Constant Frequency)

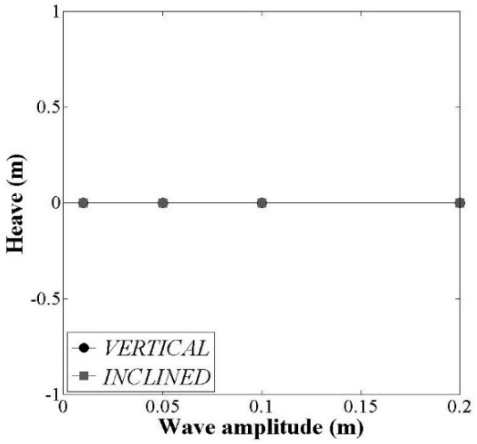

(b) Heave (Constant Frequency)

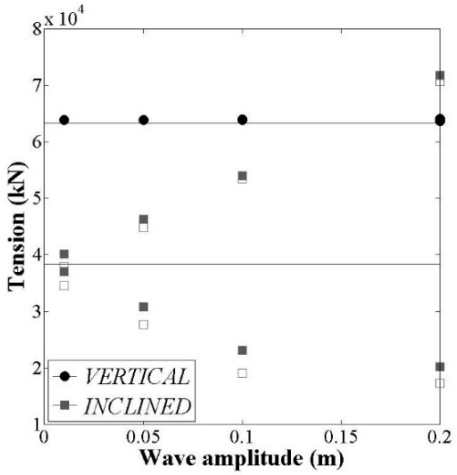

(c) Mooring tension (Constant Frequency)

Figure 5.8 (a) Surges, (b) heaves, and (c) mooring tensions of the vertically and incline moored SFTs as a function of an amplitude and at a frequency of 0.5Hz. (Open markers represent OrcaFlex and solid markers indicate CHARM3D.)

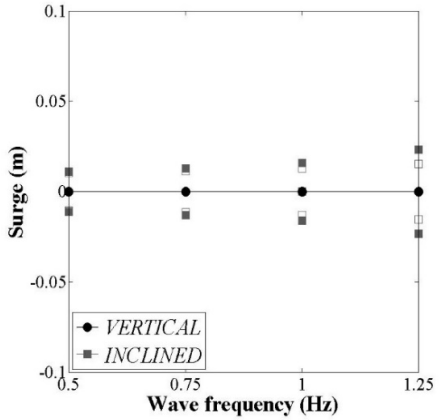

(a) Surge (Constant Amplitude)

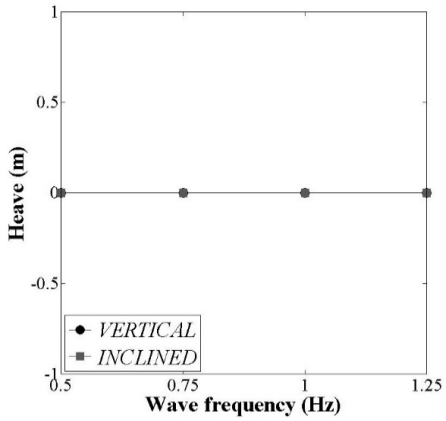

(b) Heave (Constant Amplitude)

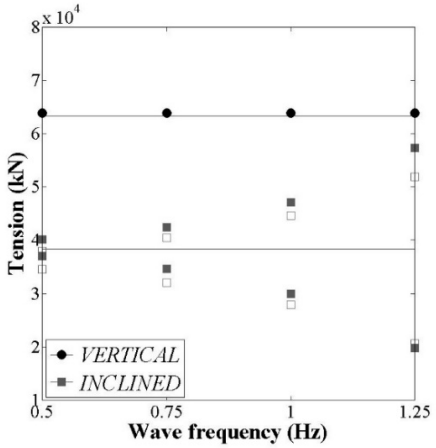

(c) Mooring tension (Constant Amplitude)

Figure 5.9 (a)Surges, (b) heaves, and (c) mooring tensions of the vertically and incline moored SFTs as a function of a frequency and at an amplitude of 0.01m. (Open markers represent OrcaFlex and solid markers indicate CHARM3D.)

5.3.2 Effects of real seismic motion

The objective of this research step was to examine the seismic responses of the SFTs relating to real seismic motion. As illustrated in Figures 4.2 and 4.4, horizontal and vertical seismic ground components were applied to the SFTs. The dynamic responses associated with real seismic excitation's effects on both their horizontal and vertical components are shown in Figures 5.10, 5.11, 5.12, and 5.13.

The first applied component was derived by the horizontal (with the seabed) surge motion of an SFT. The seismic responses illustrated in Figure 5.10 demonstrate that when subjected to the real horizontal seismic motion illustrated in Figure 4.2, the tendency of the surge motion was the same as when linear seismic motion was applied. The maximum displacement responses of both SFTs were acquired by different increases in simulated seismic motion of the following magnitudes: 3.9, 4.9, 5.4, and 6.8. Based on the time series of both types of SFT, the two different numerical simulations perfectly coincided with one another with regards to the vertical mooring configuration (see Figure 5.11); the results of the inclined mooring configuration were in agreement and had the same peak motion, even if not of an identical vertical mooring configuration (see Figure 5.12). The dynamic response of the incline moored SFT indicated that the maximum surge displacement was greater than that of the vertically moored SFT, as shown in Figure 5.1. Importantly, the motion of the inclined mooring line was magnified several times with respect to the peak response of the real horizontal seismic motion applied. The heave displacement was determined by finding the vertical difference between the corresponding point of the tunnel and the origin; the values indicated relatively little motion. The maximum mooring

line tension of the vertically moored SFT, which tended to be constant regardless of the horizontal earthquake magnitude, was remarkably larger than that of the inclined mooring line. The one exception was the significant magnitude earthquake, M6.8, because vertical mooring lines are unable to effect a 1:1 transfer of horizontal ground motion (see Figure 5.10).

Conversely, the incline moored SFT's topmost mooring tension saw a substantial increase as the magnitude of the horizontal earthquake grew larger, because inclined mooring lines exert more direct control on an SFT. When the tension force of a single line under seismic motion was compared with the results in irregular wave conditions, the tension force of the incline moored SFT at the largest seismic situation, M6.8, was similar to the tension under extreme irregular wave conditions (see Figure 5.10 and Table 5.1). However, seismic motions more devastating than the magnitude 6.80 applied in this research do occur in the world. Thus, while in general seismic excitation does not result in serious movement, the dynamic tensions in the mooring lines could have a substantially negative effect. Seismic activity that supersedes a magnitude of 6.8 occurs frequently in seismically active areas. In such situations, the dynamic response of the SFT structure and mooring line tension force are significant considerations when determining the feasibility of a submerged floating tunnel.

The time series of the surge, heave, and mooring tension and the amplitude spectrum of both SFTs are shown in Figures 5.11 and 5.12; the horizontal seismic motion was of a magnitude 6.8. For both mooring cases, the results produced by OrcaFlex coincided well with those of CHARM3D. The mooring tension of a vertically moored SFT

was very small, while the tension of an incline moored SFT was dominant, as discussed above. In terms of surge direction, the vertically moored SFT was weaker than the SFT with inclined mooring; the result was that the vertically moored SFT's surge frequencies were lower than those of the incline moored tunnel. These numerical simulations of SFT responses in earthquake conditions were designed with free end conditions. If both ends were tethered with relatively little span, the dynamic mooring tension of the incline moored SFT would increase and the outcome would be more serious. When substituted for a longer span, the resulting elastic flexibility might ameliorate some of the negative repercussions.

For comparison purposes, the dynamic behavior of an SFT when real vertical seismic ground motion is employed to the anchor points of the tunnel is plotted in Figure 5.13. The energy density spectrum of the resulting surge motion is shown in Figures 5.14 and 5.15. In seismic ground motion conditions of a vertical direction, small amounts of heave motion were more prevalent than surge motion in both vertically and incline moored SFTs. However, regardless of the magnitude of the earthquake, the mooring line tension force of an SFT with vertical mooring was substantially larger than what the results indicated for an SFT with inclined mooring. Even though the mooring tension of the vertical mooring line remained stable for horizontal seismic ground motion regardless of the magnitude, it increased with vertical seismic ground motion. At a magnitude of 6.8, the effective tension force of the vertically moored SFT under vertical seismic motion was almost 25% larger than when horizontal seismic motion was applied. Therefore, the results demonstrate that the effects of horizontal seismic ground motion are more dominant than

vertical ground motion with regards to the dynamic movement of an SFT. Furthermore, when the horizontal and vertical seismic motions (M6.8) were applied simultaneously, which is the closest to real-world conditions, the strongest mooring tensions were similar under both horizontal and vertical ground motion conditions.

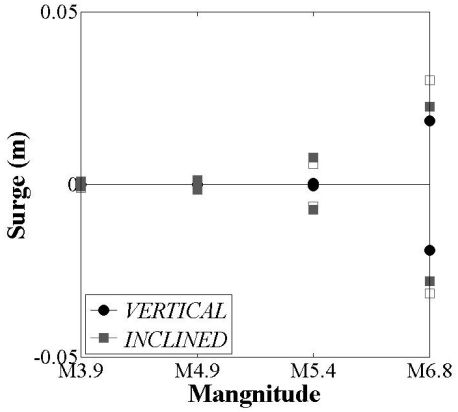

(a) Surge

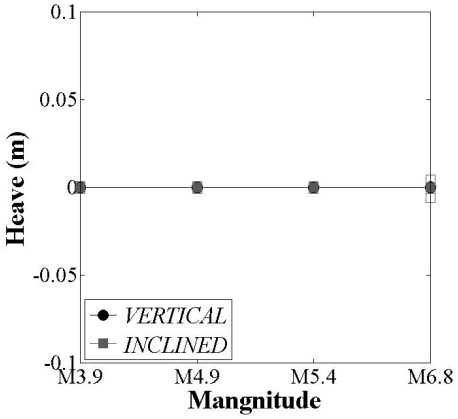

(b) Heave

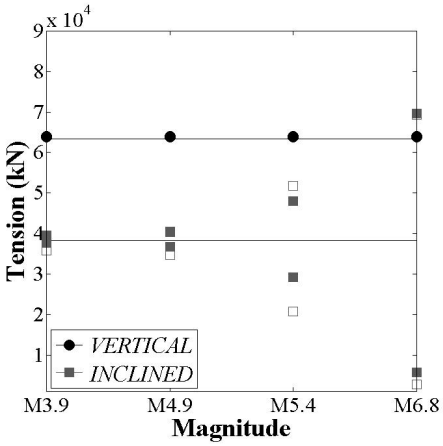

(c) Mooring tension

Figure 5.10 Numerical results for the (a) surges, (b) heaves, and (c) tensions of vertical and inclined mooring lines under real horizontal seismic motion. (Open markers represent OrcaFlex and solid markers indicate CHARM3D.

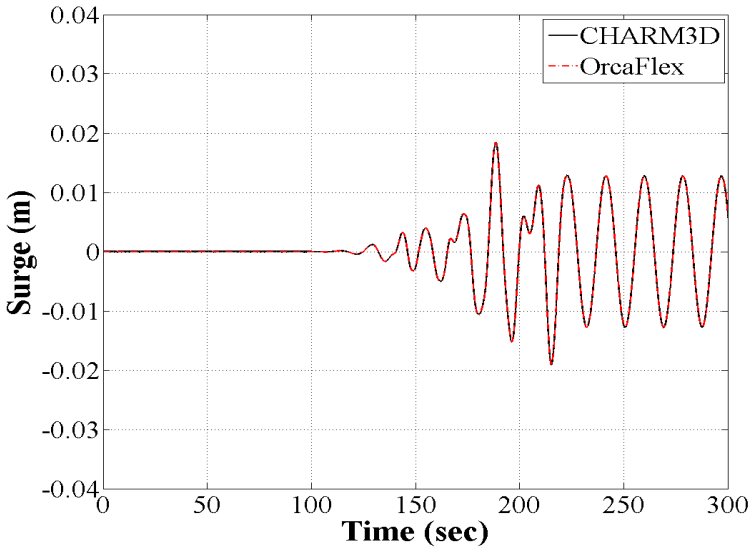

(a) WNW of Ferndale, California
(Magnitude = 6.8)

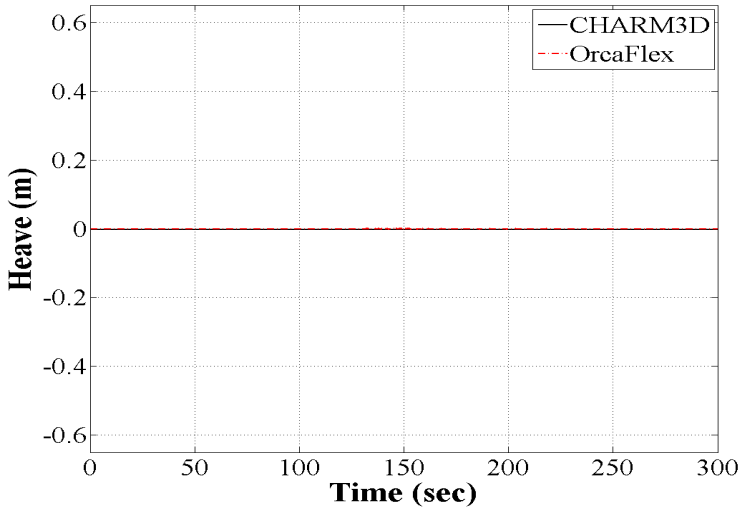

(b) WNW of Ferndale, California
(Magnitude = 6.8)

Figure 5.11 Numerical results for the (a) surge, (b) heave, (c) tension, and (d) energy density spectrum of a vertical mooring line responding to horizontal seismic components.

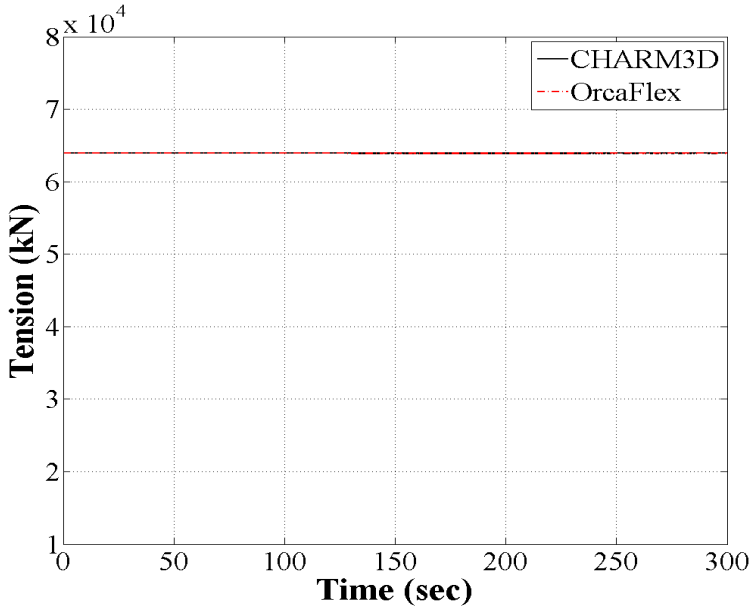

(c) WNW of Ferndale, California
(Magnitude = 6.8)

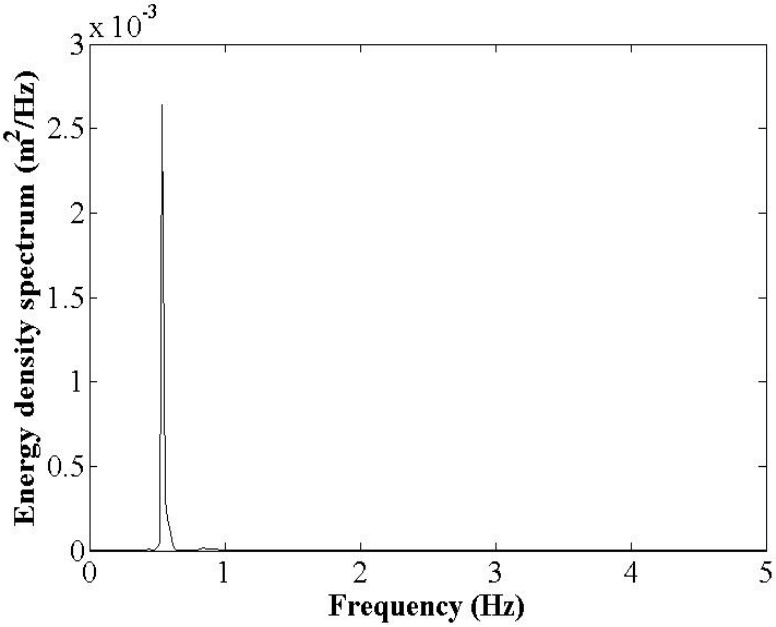

(d) WNW of Ferndale, California
(Magnitude = 6.8)

Figure 5.11 continued

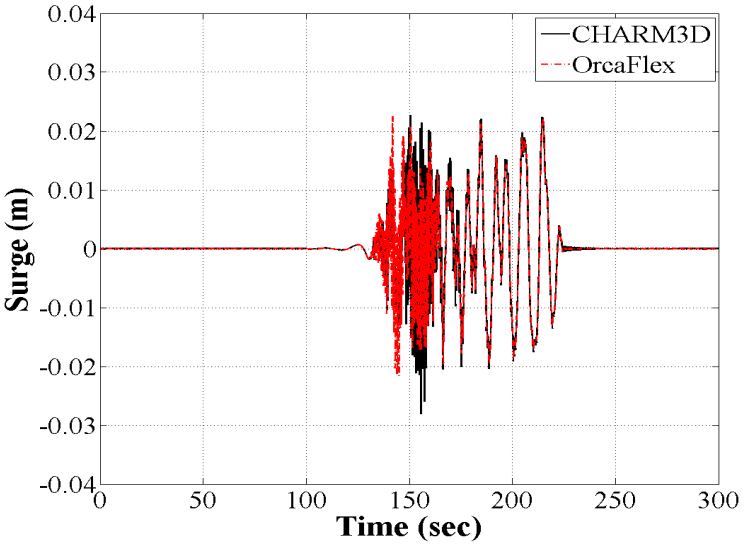

(a) WNW of Ferndale, California
(Magnitude = 6.8)

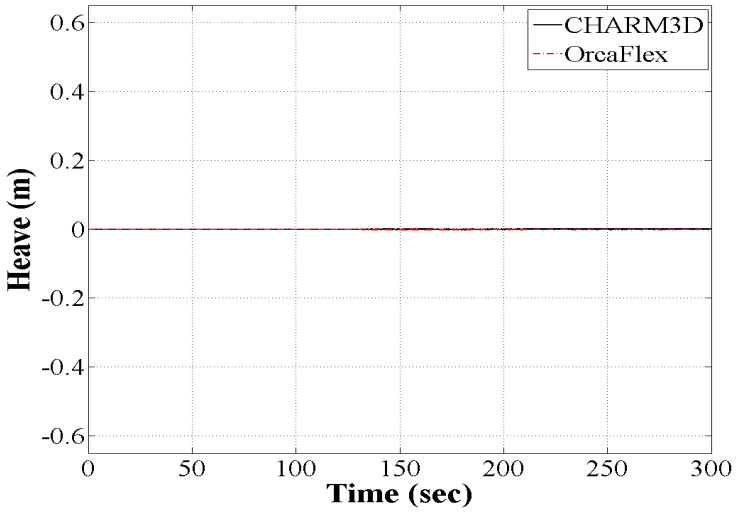

(b) WNW of Ferndale, California
(Magnitude = 6.8)

Figure 5.12 Numerical results for the (a) surge, (b) heave, (c) tension, and (d) energy density spectrum of an inclined mooring line responding to horizontal seismic components.

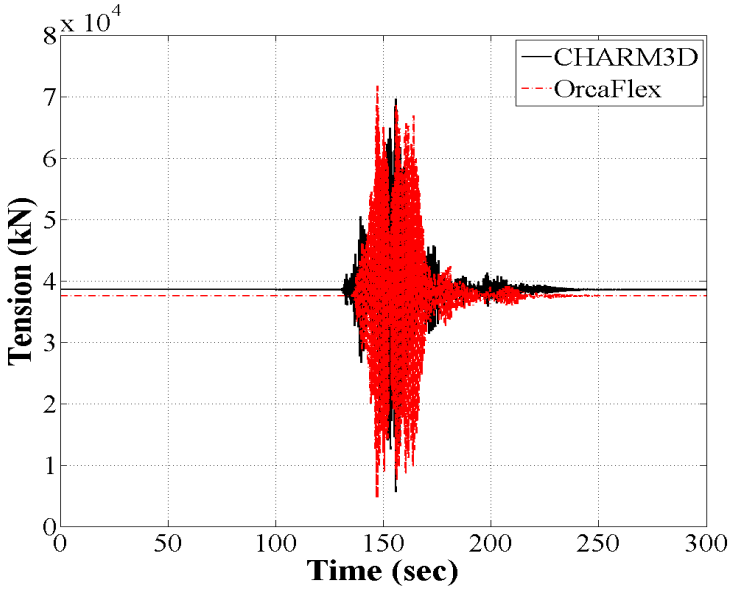

(c) WNW of Ferndale, California
(Magnitude = 6.8)

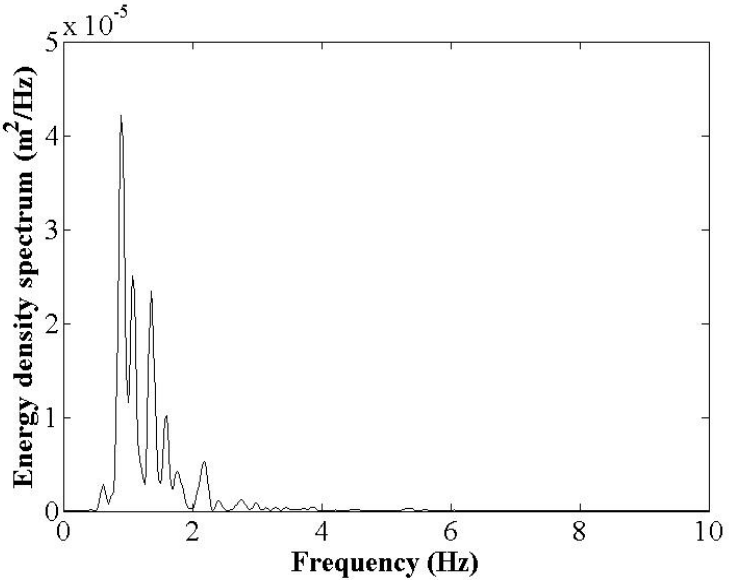

(d) WNW of Ferndale, California
(Magnitude = 6.8)

Figure 5.12 continued

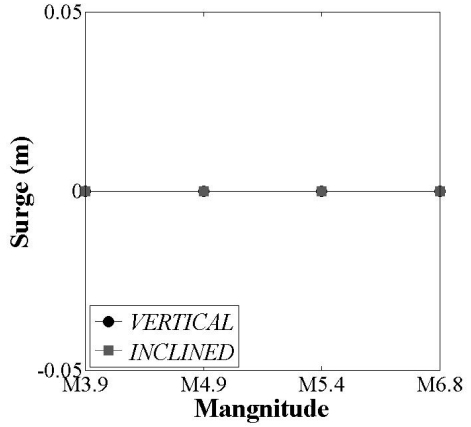

(a) Surge

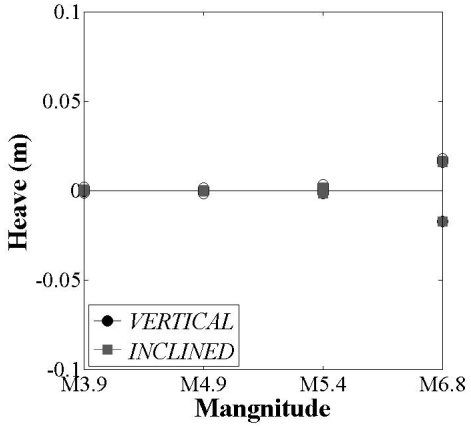

(b) Heave

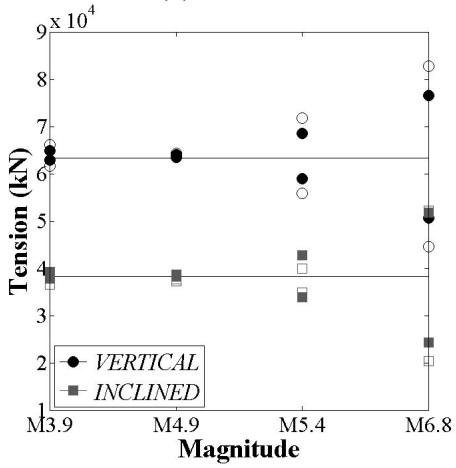

(c) Mooring tension

Figure 5.13 Numerical results for the (a) surges, (b) heaves, and (c) tensions of vertical and inclined mooring lines under real vertical seismic motion conditions. (Open markers represent OF and solid markers denote CP.)

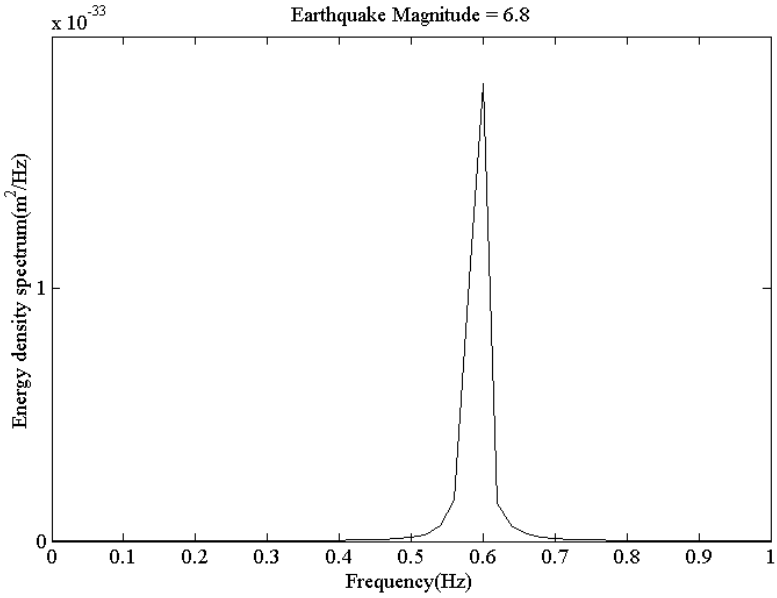

Figure 5.14 Energy density spectrum of a vertical mooring line responding to vertical seismic components.

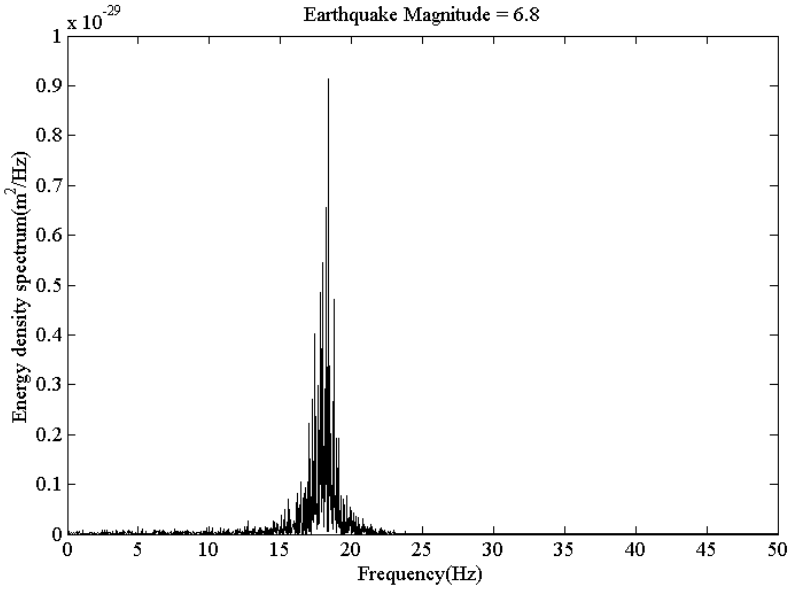

Figure 5.15 Energy density spectrum of an inclined mooring line responding to vertical seismic components.

CHAPTER VI

CONCLUSION

In this study, the dynamic responses of SFTs to hydrodynamic and seismic loads were analyzed using numerical simulations produced in OrcaFlex and CHARM3D. The dynamic motion of an SFT with a rigid body structure and free ends was the sole focus of this research; thus, the effects of fluid compressibility induced by seismic motion for global dynamics were excluded. Based on the validation of the SFT models under regular wave conditions, this study investigated the dynamic behaviors of SFTs in response to irregular waves and seismic motion (both horizontal and vertical seismic ground movement). The main results revealed the surge and heave motions of the SFTs, as well as their mooring tension. The principal effects of waves and seismic motion on SFT systems were then investigated and compared via two different simulations. Using OrcaFlex, the hydrodynamic loads were calculated according to the Wheeler stretching method, and four real seismic motions were employed to examine the SFTs' seismic behaviors. The numerical results obtained from the two different software packages were then compared to the experimental data from Oh et al. (2013), in order to validate the approach used in this study.

Overall, the results of the numerical simulation coincided with the laboratory data under regular wave conditions. Furthermore, the outcomes of the two simulations were in agreement with one another under both irregular wave and seismic conditions. SFTs are usually installed at deep sea depths, so they are not affected by short waves or low to

medium intensity sea conditions. While the vertically moored SFT presented an enormous dynamic response, particularly in regular waves with long wave periods and extremely irregular wave conditions, under extreme hydrodynamic conditions, the incline moored SFT effectively restricted both surge and heave motions. Even though the effective tension of the single mooring line for the vertical mooring configuration was larger than that of the SFT with inclined mooring, the total effective tension of the inclined mooring line was larger than that of the vertical mooring line; this was attributable to the increased number of mooring lines that this mooring configuration required. Relatedly, the difference between the two numerical simulations was likely caused by the difference in drag coefficient and use of the Wheeler stretching method.

In contrast to hydrodynamic conditions, when ground seismic motion in a horizontal direction was applied, the SFT with inclined mooring presented the dominant dynamic response. Moreover, while the dynamic responses of the SFTs were small compared to their simulations under hydrodynamic conditions, the dynamic mooring tensions of the SFTs under seismic motion could be substantially amplified. The dynamic motion trend of the SFTs under seismic motion was that the incline moored SFT followed the applied seismic motion. However, the total effective tension of the inclined mooring line design was greater than that of the vertical mooring design. In this situation, the tension of a single inclined mooring line increased with an increase in seismic magnitude when horizontal seismic motion was employed. Also, the tension of the inclined mooring line in the final, largest seismic event was similar to the results under extreme irregular wave conditions. Thus, under a seismic impact of significant magnitude, mooring line

tension is a significant design factor because the effective tension is directly proportional to the seismic magnitude. Conversely, in terms of vertical seismic components, the dynamic motions of both SFTs were almost negligible when compared to the results produced by horizontal seismic components.

Overall, by comparing the results from the two types of SFTs under different environmental conditions, it can be concluded that the incline moored SFT design offers a better performance with respect to hydrodynamic loads than the vertical mooring line design. However, in seismic conditions, vertical mooring is more stable than inclined mooring. When earthquake frequencies approach the normal frequencies of mooring movement and general SFT motion, conditions can become more hazardous. Consequently, the results presented herein illustrate the design potential of this type of submerged floating tunnel, and provide valuable information to the future advancement of this type of design.

REFERENCES

Brancaleoni, F., A. Castellani, and P. D'asdia. (1989). "The response of submerged tunnels to their environment." *Engineering Structures, 11*(1), 47-56.

Chen, W., and Huang, G. (2010). "Seismic wave passage effect on dynamic response of submerged floating tunnels." *Procedia Engineering, 4*, 217-224.

Cheng, X., Xu, W., Yue, C., Du, X., and Dowding, C. H. (2014). "Seismic response of fluid–structure interaction of undersea tunnel during bidirectional earthquake." *Ocean Engineering*, *75*, 64-70.

Chopra, Anil K. (2007). Dynamics of structures: theory and applications to earthquake engineering. 3 rd ed. Upper Saddle River, NJ: Pearson/Prentice Hall, Print.

Cifuentes, C., Kim, S., Kim, M. H., and Park, W. S. (2015). "Numerical simulation of the coupled dynamic response of a submerged floating tunnel with mooring lines in regular waves." *Ocean Systems Engineering, 5*(2), 109-123.

Dean W.R. (1948). "On the reflection of surface waves by a submerged cylinder." *Mathematical Proceedings of the Cambridge Philosophical Society*. *44*(4), 483-491.

DeCew, J., Tsukrov, I., Risso, A., Swift, M. R., and Celikkol, B. (2010). "Modeling of dynamic behavior of a single-point moored submersible fish cage under currents," *Aquac. Eng.*, *43*(2), 38–45.

Di Pilato, M., Perotti, F., and Fogazzi, P. (2008). "3D dynamic response of submerged floating tunnels under seismic and hydrodynamic excitation." *Engineering Structures, 30*(1), 268-281.

Fogazzi, P. and F. Perotti. (2000). "The dynamic response of seabed anchored floating tunnels under seismic excitation." *Earthquake Engineering & Structural Dynamics*, *29*(3), 273-295.

Garrett, D. L. (1982). “Dynamic analysis of slender rods.” *Journal of Energy Resources Technology*, *104*(4), 302-306.

Haritos, N. and He, D. T. (1992). “Modelling the response of cable elements in an ocean environment.” *Finite Elem. Anal. Des.*, *11*, 19–32.

Hyun C.H., Yun C.B., and Lee D.G. (1992). “Nonstationary response analysis of a suspension bridge for multiple support excitations.” *Probabilistic Engineering Mechanics*, *7*(1), 27–35.

Kim, M. H., Koo, B. J., Mercier, R. M., and Ward, E. G. (2005). “Vessel/mooring/riser coupled dynamic analysis of a turret-moored FPSO compared with OTRC experiment.” *Ocean Eng., 32*(14–15), 1780–1802.

Kunisu, H. (2010). “Evaluation of wave force acting on submerged floating tunnels.” *Procedia Eng., 4*, 99–105.

Lee, J. H., Seo, S. I., Mun, H. S. (2016). “Seismic behaviors of a floating submerged tunnel with a rectangular cross-section.” *Ocean Engineering, 127*, 32-47.

Lee, J. Y., Jin, C. K., Kim, M. H. (2017). “Dynamic response analysis of submerged floating tunnels by wave and seismic excitation.” *Ocean System Engineering*, 7(1).

Maruo H. (1957). “The excess resistance of a ship in rough seas.” *Int Shipbuild Prog*, *4*(35), 337e45.

Mirzapour, J., M. Shahmardani, and S. Tariverdilo. (2016). "Seismic response of submerged floating tunnel under support excitation." *Ships and Offshore Structures*, 1-8.

Oh, S.H., Park, W.S., Jang, S.C., Kim, D.H. and Ahn, H.D. (2013). “Physical experiments on the hydrodynamic response of submerged floating tunnel against the wave action.” *APAC*, 24-26.

Orcina, (2015). *OrcaFlex Manual Version 9.8a*. Ulverston, LA, Orcina.

Østlid, H. (2010). "When is SFT competitive?," *Procedia Eng.*, *4*(1877), 3–11.

Remseth, S., Leira, B.J., Okstad, K.M., Mathisen, K.M., and Haukas, T. (1999). "Dynamic response and fluid/structure interaction of submerged floating tunnels." *Computers and Structures*, *72*(4), 659–685.

Wheeler, J. D. (1969). "Methods for calculating forces produced by irregular waves." *Offshore Technology Conference*, Offshore Technology Conference, 359-367.